

# Extending the range of applicability of the semi-empirical ecosystem flux model PRELES for varying forest types and climate

Xianglin Tian<sup>1,2</sup>  | Francesco Minunno<sup>2</sup>  | Tianjian Cao<sup>1</sup>  | Mikko Peltoniemi<sup>3</sup>  |  
Tuomo Kalliokoski<sup>2,4</sup>  | Annikki Mäkelä<sup>2</sup> 

<sup>1</sup>College of Forestry, Northwest A&F University, Yangling, China

<sup>2</sup>Department of Forest Sciences, University of Helsinki, Helsinki, Finland

<sup>3</sup>Natural Resources Institute Finland, Helsinki, Finland

<sup>4</sup>Department of Physics, University of Helsinki, Helsinki, Finland

## Correspondence

Tianjian Cao, College of Forestry, Northwest A&F University, Yangling 712100, China.  
Email: cao@nwafu.edu.cn

## Funding information

National Natural Science Foundation of China, Grant/Award Number: NSFC 31670646; Academy of Finland, Grant/Award Number: 286190; Strategic Research Council at the Academy of Finland, Grant/Award Number: 312635 and 312912; Horizon 2020 Research and Innovation Framework Program, Grant/Award Number: 821860

## Abstract

Applications of ecosystem flux models on large geographical scales are often limited by model complexity and data availability. Here we calibrated and evaluated a semi-empirical ecosystem flux model, PREdict Light-use efficiency, Evapotranspiration and Soil water (PRELES), for various forest types and climate conditions, based on eddy covariance data from 55 sites. A Bayesian approach was adopted for model calibration and uncertainty quantification. We applied the site-specific calibrations and multisite calibrations to nine plant functional types (PFTs) to obtain the site-specific and PFT-specific parameter vectors for PRELES. A systematically designed cross-validation was implemented to evaluate calibration strategies and the risks in extrapolation. The combination of plant physiological traits and climate patterns generated significant variation in vegetation responses and model parameters across but not within PFTs, implying that applying the model without PFT-specific parameters is risky. But within PFT, the multisite calibrations performed as accurately as the site-specific calibrations in predicting gross primary production (GPP) and evapotranspiration (ET). Moreover, the variations among sites within one PFT could be effectively simulated by simply adjusting the parameter of potential light-use efficiency (LUE), implying significant convergence of simulated vegetation processes within PFT. The hierarchical modelling of PRELES provides a compromise between satellite-driven LUE and physiologically oriented approaches for extrapolating the geographical variation of ecosystem productivity. Although measurement errors of eddy covariance and remotely sensed data propagated a substantial proportion of uncertainty or potential biases, the results illustrated that PRELES could reliably capture daily variations of GPP and ET for contrasting forest types on large geographical scales if PFT-specific parameterizations were applied.

## KEYWORDS

evapotranspiration, geographical variations, gross primary production, inverse modelling, light-use efficiency, multisite calibration, plant functional type

## 1 | INTRODUCTION

One of the major problems in the applications of ecosystem models and physiological models is the level of complexity (Landsberg & Sands, 2011). Models concerning detailed physiological mechanisms or ecosystem processes can theoretically be extrapolated to new sites or to future climates, but appropriate input data and parameters are often difficult to obtain (Landsberg, 2003; Mäkelä et al., 2000), despite the profound development of physiological measurement equipment during last decades. Simplified models are less data-demanding with fewer parameters, but usually extrapolate poorly and may overlook crucial interactions of the ecosystems (Monserud, 2003; Weiskittel, Hann, Kershaw, & Vanclay, 2011). Therefore, in applying models on a larger geographical scale or under changing environmental conditions, it is always necessary to recalibrate the models or test their applicability. Due to improved measurement techniques and automated data-recording systems, numerous databases such as eddy flux, soil property and species distribution are becoming available to fulfil the need for detailed information on stand characteristics or dynamics. For instance, remotely sensed estimates such as canopy light interception, measured as the fraction of absorbed photosynthetically active radiation ( $f_{\text{APAR}}$ ), could determine the spatial variation of input for ecosystem models (Waring, Coops, & Landsberg, 2010). Meanwhile, inverse modelling approaches, such as Bayesian calibration (BC), adjust model parameters and processes according to their ability to reproduce stand-level field observations, which bridges the gap between complex models and various databases (e.g. Hartig et al., 2012; Van Oijen, Rougier, & Smith, 2005). By combining these data and modelling approaches, it is possible to test or extend the applicable ranges of ecosystem models that were originally developed for small-scale regions.

Gross primary production (GPP), the sum of the net photosynthesis by all photosynthetic tissue measured at the ecosystem scale, is a key factor in the ecosystem carbon balance. It is the original carbon source for all the forest ecosystem carbon fluxes. Measurements and simulations of GPP help us to understand the development of forest ecosystem and its interactions with climate. Benefited from the rapid development of the eddy covariance network during recent decades (Aubinet, Vesala, & Papale, 2012), both empirical and semi-empirical canopy GPP models can be calibrated and validated sufficiently. Empirical ecosystem flux models have been applied to explain distinctions in productivity between sites or vegetation types (e.g. Falge et al., 2002). Furthermore, satellite-driven LUE approaches have been frequently used for monitoring geographical variation of ecosystem productivity (e.g. Potter et al., 1993; Sims et al., 2008; Yuan et al., 2007). The trade-off of model simplicity is that much of the ecosystem variation remains unexplained (Yuan, Cai, Xia, et al., 2014; Zheng et al., 2018), although the data requirement of those models can be globally fulfilled. Semi-empirical canopy GPP models have commonly been used as a submodule of process-based models, such as the photosynthesis modules of 3-PG (Landsberg & Waring, 1997), PnET-II (Aber & Federer, 1992) and FOREST-BGC (Running & Coughlan, 1988). Instead of reducing the data requirement, those

models rely on the adequacy of the underlying physiological assumptions, extending the applicability of the model to all stands where the physiological parameters can be evaluated.

PREdict Light-use efficiency, Evapotranspiration and Soil water (PRELES) is a semi-empirical ecosystem flux model that predicts daily GPP, evapotranspiration (ET) and soil water (Peltoniemi, Pulkkinen, et al., 2015). The model requires soil characteristics, daily  $f_{\text{APAR}}$  and meteorological observations as inputs. The GPP predictions are based on a reformulation of the light-use efficiency (LUE) model of Mäkelä et al. (2008). PRELES has been calibrated and validated in the boreal region mainly for coniferous forests (Minunno et al., 2016; Peltoniemi, Pulkkinen, et al., 2015; Peltoniemi et al., 2012). When national inventory and map data were available, PRELES predicted GPP estimates in Finland similar to those of the model JSBACH and MODIS GPP product (MOD17), although the input data sources differed (Peltoniemi, Markkanen, et al., 2015). Linked with down-scaled global circulation model projections, PRELES has been used to predict boreal forest productivity under climate change scenarios, and its parametric uncertainty is marginal when compared with other sources of uncertainty (Kalliokoski, Mäkelä, Fronzek, Minunno, & Peltoniemi, 2018). Furthermore, PRELES has been linked with a process-based carbon allocation model CROBAS (Mäkelä, 1997; Valentine & Mäkelä, 2005) in simulating forest variables with a country-generic calibration in Finland (Minunno et al., 2019). Mäkelä et al. (2008) showed that daily temperature, vapour-pressure deficit (VPD) and absorbed photosynthetic photon flux density (PPFD) accounted for most of the daily variation in GPP in the model, but unexplained variation remained in the site-specific maximum LUE, which correlated linearly with canopy nitrogen (Peltoniemi et al., 2012). When the model was fitted to data, differences between sites could be explained by potential LUE, leaf area and environmental conditions. For wider applications, the ability of the model to extrapolate to conditions outside the original modelling sites must be evaluated. Minunno et al. (2016) tested the applicability of PRELES for 10 boreal coniferous forests in Fennoscandia and obtained a generic vector of model parameters by multisite calibration. Based on a comparison between site-specific and multisite calibration, the generic parameter vector from multisite calibration can be reliably used at the regional scale for boreal coniferous forests. However, in this multisite calibration, all the sites were coniferous forests and shared the same parameters, thus omitting the differences in potential LUE by site fertility or species range. Incorporating the processes of light saturation, temperature acclimation, VPD stress and soil water dynamics, PRELES is theoretically qualified for monitoring and predicting ecosystem productivity of various forest-climate types, but this wide range of applicability has not been tested in warmer climate types, broad-leaved forests or very fertile soils.

The objectives of the study were: (a) to test, with additional modules of seasonality and water dynamics incorporated, whether the LUE approach could sufficiently explain geographical variations of GPP and ET, with respect to contrasting environmental conditions and distinctive forest ecosystems; (b) to propose a generic parameter vector for each plant functional type (PFT) and to hierarchically

quantify the differences among sites while fitting the model with pooled data; and (c) to quantify the uncertainty in extrapolating to conditions outside the original sites.

## 2 | MATERIALS AND METHODS

### 2.1 | Framework of PRELES

PREdict Light-use efficiency, Evapotranspiration and Soil water is a semi-empirical ecosystem flux model that predicts daily GPP ( $P$ , g C m<sup>-2</sup> day<sup>-1</sup>), ET ( $E$ , mm/day) and soil water (mm). The requirements of site-specific inputs include the soil depth exploited by the roots (mm), field capacity (mm) and wilting point (mm) of the soil,  $f_{\text{APAR}}$ , and daily meteorological observations that include the PPFD (mol m<sup>-2</sup> day<sup>-1</sup>) above the canopy, air temperature (°C), VPD (kPa) and precipitation (mm/day). A detailed description of PRELES can be found in Peltoniemi, Pulkkinen, et al. (2015), and the code applied in this study is provided in the GitHub repository (<https://github.com/ForModLabUHel/Rprebas>). Here, we introduce a brief framework of the  $P$  and  $E$  submodels. Daily photosynthetic production during day  $k$ ,  $P_k$ , is predicted as follows:

$$P_k = \beta \cdot \phi_k \cdot f_{\text{APAR},k} \cdot f_{L,k} \cdot f_{S,k} \cdot \min(f_{D,k}, f_{W,P,k}) \cdot f_{\text{CO}_2,P,k} \quad (1)$$

where  $\beta$  is the potential LUE (g C/mol),  $\phi_k$  the PPFD (mol m<sup>-2</sup> day<sup>-1</sup>) and  $f_{\text{APAR}}$  the fraction of  $\phi_k$  absorbed by the canopy during day  $k$ . The  $f_{L,k}$ ,  $f_{S,k}$ ,  $f_{D,k}$  and  $f_{W,P,k}$  constrained between 0 and 1, are respectively the modifiers that account for the suboptimal conditions in light  $L$ , temperature acclimation  $S$ , VPD ( $f_{D,k}$ ), and soil-water stress  $W$  ( $f_{W,P,k}$ ). The explanations of these modifiers can be found in Mäkelä et al. (2008). The modifier  $f_{\text{CO}_2,P,k}$  accounts for the impact of ambient CO<sub>2</sub> concentration on photosynthesis (for details see Kallioikoski et al., 2018). The daily ET during day  $k$ ,  $E_k$ , is simulated as follows:

$$E_k = \alpha \cdot P_k \cdot f_{W,P,k}^\nu \cdot D_k^{1-\lambda} + \chi \cdot (1 - f_{\text{APAR},k}) \cdot \phi_k \cdot f_{W,E,k} \cdot \frac{s_{\text{DS},k}}{s_{\text{DS},k} + p_{\text{psychrom}}} \quad (2)$$

where  $\alpha$  is a transpiration parameter,  $\chi$  an evaporation parameter and  $\lambda$  an adjustment parameter for the effect of  $D$  on transpiration during day  $k$ . The  $f_{W,P,k}$  is raised to the power  $\nu$ , since the response of  $E_k$  to soil-water stress may differ from that of  $P_k$ . Another modifier,  $f_{\text{CO}_2,E,k}$  was adopted to replace  $f_{\text{CO}_2,P,k}$  in Equation (1) when calculating the impact of the CO<sub>2</sub> concentration on transpiration (Kallioikoski et al., 2018). The modifier  $f_{W,E,k}$  accounts for the suboptimal condition of evaporation due to soil water, while  $s_{\text{DS},k}$  is the slope of the relationship between the saturation vapour pressure (kPa) and air temperature (°C), and  $p_{\text{psychrom}}$  is the psychrometric constant (Campbell, 1977) that relates the partial pressure of water in air to the air temperature (kPa/°C).

PREdict Light-use efficiency, Evapotranspiration and Soil water has 20 parameters (Table 1) and only two state variables (Peltoniemi, Pulkkinen, et al., 2015). One state variable is soil water content, and the other is the state of temperature acclimation. The soil water

balance module simulates the ecosystem as a bucket being filled by precipitation and emptied by drainage and ET. The state of temperature acclimation considers adaptive strategies of plants by simulating the slow response of photosynthesis to changes in ambient temperature. A table listing the symbols with their units and meanings is given in Table S2, including model input, output, estimated variables, parameters and mathematical symbols.

### 2.2 | Data

#### 2.2.1 | Eddy covariance data

The meteorological and eddy covariance data were maintained and shared by the FLUXNET community. Daily meteorological and flux records of 399 site-years from 55 sites (Figure 1) were selected and downloaded from the 'FLUXNET2015 dataset', in which half-hourly observations were gap-filled, aggregated and transformed to daily records by a standard methodology (Papale et al., 2006; Reichstein et al., 2005). Records of GPP were not directly measured but inferred from the net ecosystem exchange (NEE) of CO<sub>2</sub> using the nighttime data-based partitioning method. The partitioning methodology has been validated for various climate and PFTs (Reichstein et al., 2005) and implemented in FLUXNET following a standard protocol. Further detailed information on the FLUXNET sites used in model calibration is given in Table S1. Various forest and climate types were considered in our study, ranging from tropical broad-leaved forests to cold continental coniferous forests.

The daily meteorological observations of the data set constituted the input variables for PRELES. In addition, the daily eddy covariance records of GPP and ET were used for comparing with the model outputs. The daily records were originally generated uniformly from half-hourly observations. A quality flag, constrained between 0 and 1, was assigned to each day to indicate the proportion of measured (nongap-filled) and good quality gap-filled half-hourly data used to calculate the daily value. For the calibration and analysis conducted in this study, we used only data with a quality flag higher than 0.7.

#### 2.2.2 | MODIS $f_{\text{APAR}}$ data

The daily time series of  $f_{\text{APAR}}$  throughout the growing season were collected from remotely sensed data products from the Moderate Resolution Imaging Spectroradiometer (MODIS) collections (ORNL DAAC 2008, 2017). The product MOD15A2 is an 8 day 1 km resolution product on a sinusoidal grid (Myneni, Knyazikhin, & Park, 2015a), and the product MOD15A2H is an 8 day composite data set with 500 m pixel size (Myneni, Knyazikhin, & Park, 2015b). We chose data from Terra (MOD) instead of Aqua (MYD) or the combined product (MCD), since the time of the Terra overpass (about 10:30 a.m.) is a better approximation of the daily integrated black sky (i.e. assuming only direct radiation from the sun)  $f_{\text{APAR}}$  (Martínez, Camacho, Verger, García-Haro, & Gilabert, 2013). A simple harmonic

TABLE 1 Parameters in PRELES

Symbol	Meaning	Units	Prior minimum	Prior maximum	Included in site-specific calibration?	Included in multisite calibration?
$\chi$	Evaporation parameter	dm <sup>3</sup> /mol	0	2.5	Yes	Yes
$\gamma$	Light modifier parameter for saturation with irradiance	mol <sup>-1</sup> m <sup>-2</sup>	1.03e-4	0.503	Yes	Yes
$\alpha$	Transpiration parameter	mm (g C m <sup>-2</sup> kPa <sup>1-<math>\alpha</math>)<sup>-1</sup></sup>	1e-6	10	Yes	Yes
$X_0$	Threshold for state of acclimation change	°C	—	—	Yes	Yes
$\beta$	Potential light-use efficiency	gC/mol	0.2	2.5	Yes	Yes
$S_{\max}$	Threshold above which the acclimation modifier reaches its maximum	°C	—	—	Yes	Yes
$\lambda$	Parameter adjusting water-use efficiency with vapour-pressure deficit	—	1e-4	0.999	Yes	Yes
$\rho_p$	Threshold for the effect of soil-water stress on photosynthesis	—	0	0.999	Yes	Yes
$\nu$	Parameter adjusting water-use efficiency whether soil water limits gross primary production	—	1e-4	2.5	Yes	Yes
$\kappa$	Sensitivity parameter for vapour-pressure deficit response	kPa <sup>-1</sup>	-1	-1e to 3	Yes	Yes
$\rho_E$	Threshold for the effect of soil-water stress on evaporation	—	0	0.999	Yes	Yes
$\tau$	Delay parameter for ambient temperature response	—	1	25	Yes	Yes
$D_{\text{soil}}$	Effective depth of soil that excludes stones and can be explored by plant roots	mm	—	—	Yes	No
$\theta_{\text{FC}}$	Effective field capacity	mm	—	—	Yes	No
$\theta_{\text{WP}}$	Effective wilting point	mm	—	—	Yes	No
$\theta_{\text{surf,max}}$	Maximum of the water storage on canopy surface	mm	0.5	10	Yes	No
$\tau_F$	Delay parameter of drainage	—	1	5	Yes	No
$p_{\text{GPP}}$	Parameter adjusting the effect of ambient CO <sub>2</sub> concentration on photosynthesis	—	—	—	No	No
$p_{\text{ET}}$	Parameter adjusting the effect of ambient CO <sub>2</sub> concentration on transpiration	—	—	—	No	No
$m$	Coefficient for temperature dependence of snowmelt rate	°C <sup>-1</sup> day <sup>-1</sup>	—	—	No	No

Note: The 12 parameters in multisite calibration are ordered by their sensitivity to the model outputs (Peltoniemi, Pulkkinen, et al., 2015). The minimum and maximum values of  $X_0$  and  $S_{\max}$  are adjusted, based on the seasonal temperature ranges at each site or of each plant functional type. The ranges of prior for soil-related parameters were set separately for each site based on information from global data sets. The reasons for exclusion of  $p_{\text{GPP}}$  and  $p_{\text{ET}}$  from calibration are given in Section S3. Coefficient  $m$  was set as a constant according to Kuusisto (1984).

Abbreviations: GPP, gross primary production; PPFD, photosynthetic photon flux density; PRELES, PREDict Light-use efficiency, Evapotranspiration and Soil water; VPD, vapour-pressure deficit.

model was constructed to simulate the temporal dynamics of (Kozlov, Kozlova, & Skorik, 2016).

$$f(t) = a_0 + \sum_{j=1}^n b_j \cos 2\pi jt + \sum_{j=2}^n c_j (\sin 2\pi jt - j \sin 2\pi t), \quad (3)$$

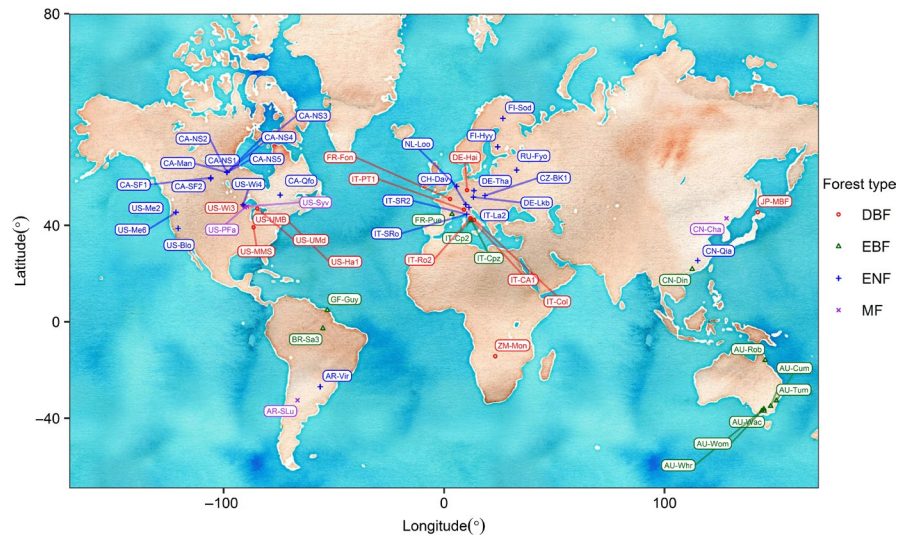
where  $f(t)$  is the  $f_{\text{APAR}}$  at time  $t$ ,  $t$  is the time in percentage normalized within the growing season,  $a_0$ ,  $b_1$ , ...,  $b_n$ ,  $c_2$ , ...,  $c_n$  are coefficients,

$n$  represents a particular number of harmonics and  $j$  is the index of summation.

### 2.2.3 | Soil information and climate classification

For each site, water-holding capacity information, including soil field capacity and soil wilting point, was collected from the Global

**FIGURE 1** Study sites. DBF, deciduous broad-leaved forest; EBF, evergreen broad-leaved forest; ENF, evergreen needle-leaved forest; MF, mixed forest



Gridded Surfaces of Selected Soil Characteristics data set (within a global 5 arcminute grid), which was developed by the Global Soil Data Task Group (2000) of the International Geosphere-Biosphere Programme Data and Information System. For soil depth, we gathered information combined from two data sets, one being the Global 1 km Gridded Thickness of Soil, Regolith and Sedimentary Deposit Layers data set (Pelletier et al., 2016), which provides high-resolution estimates of the thickness of the permeable layers above the bedrock within a global 30 arcsecond grid. Another data set is the International Satellite Land-Surface Climatology Project Initiative II Ecosystem Rooting Depths (Schenk & Jackson, 2009), which provides mean ecosystem rooting depths for  $1^\circ \times 1^\circ$  grid cells. Climate classification for all 55 sites was based on an updated world map of Köppen-Geiger climate classification within a global  $0.1^\circ$  grid (Peel, Finlayson, & McMahon, 2007). The climate classification was a crucial criterion for grouping of the sites in multisite calibration as explained in the following section.

## 2.3 | Methods

### 2.3.1 | Site-specific calibration and multisite calibration

Statistical calibration of the PRELES model parameters was accomplished in a Bayesian framework by inferring the joint posterior probability density distribution of parameters conditioned on observations (Van Oijen et al., 2005). We implemented two types of calibration: site-specific calibration and multisite calibration. The site-specific calibration included 17 parameters and was applied to each site independently (Table 1). The five parameters concerning local soil, canopy or terrain information were included in site-specific calibration but excluded in multisite calibration (Table 1). For instance, the soil depth parameter was calibrated within a  $\pm 15\%$  range, because the soil

information came from a data set with low resolution (Section 2.2.3), and soil depth varies largely with terrain attributes in reality. The records of ecosystem rooting depths were set as medians in prior settings. A higher range, for example  $\pm 30\%$ , was set when the record of the rooting depths largely differed from the soil depth data. The updated soil depth information from site-specific calibrations, the maximum a posteriori probability estimate (MAP), was directly used as input in the multisite calibrations and simulations.

For multisite calibration, we selected 50 from 55 sites and divided them into nine PFTs, based on the forest types and Köppen-Geiger climate classification (Table 2). The division excluded five sites because they belong to either mixed forests (MFs) or unique climate types (Table S1) and thus could not be classified into any group in Table 2. A generic parameter vector for each cluster was calibrated, using the Bayesian hierarchical modelling method.

### 2.3.2 | Likelihood based on the assumption of measurement uncertainty

Using eddy covariance measurements, three main characteristics were included in our likelihood function. First, the measurement error followed a double-exponential (or Laplace) distribution instead of Gaussian (Hollinger & Richardson, 2005). Second, the standard deviation of the random measurement uncertainty increased with the magnitude of the measurements (Richardson et al., 2008). This relationship can be approximated linearly, and the intercept has a wider range of variation compared with the slope (Aubinet et al., 2012). Third, both GPP and ET measurements were considered simultaneously during the calibration, but each followed its own error distribution separately. Eventually, the likelihood was written as the probability of the observation, conditional on the model output being the true value, which means that the residuals include both measurement error and

Forest-climate cluster	Description	No. of sites	FLUXNET ID
DBF_Cf	Temperate deciduous broad-leaved forests (without dry season)	2	FR-Fon, IT-PT1
DBF-Cs	Mediterranean deciduous broad-leaved forests	3	IT-CA1, IT-Col, IT-Ro2
DBF_Df	Boreal deciduous broad-leaved forests (without dry season)	7	DE-Hai, JP-MBF, US-Ha1, etc.
EBF_Am	Tropical monsoon evergreen broad-leaved forests	3	AU-Rob, BR-Sa3, GF-Guy, etc.
EBF_Cf	Temperate evergreen broad-leaved forests (without dry season)	6	AU-Cum, AU-Whr, CN-Din, etc.
EBF-Cs	Mediterranean evergreen broad-leaved forests	3	FR-Pue, IT-Cp2, IT-Cpz
ENF_Cf	Temperate evergreen needle-leaved forests (without dry season)	4	AR-Vir, CN-Qia, NL-Loo, etc.
ENF-Cs	Mediterranean evergreen needle-leaved forests	5	IT-SR2, US-Blo, US-Me2, etc.
ENF_Df	Boreal evergreen needle-leaved forests (without dry season)	17	CA-NS1, CH-Dav, FI-Hyy, etc.

**TABLE 2** Plant functional types for multisite calibration

Note: Detailed meanings of the letters in forest-climate classification are explained in Table S1.

model structure error (Van Oijen, 2017). The likelihood of the site-specific calibration was as follows:

$$\begin{aligned}
 p(\mathbf{Y}|\theta) &= p(\boldsymbol{\varepsilon} = \mathbf{Y} - \mathbf{M}(\theta)) \\
 &= \prod_{j=1}^2 \prod_{i=1}^{N_j} \frac{1}{2} \text{Exp} \left( |\varepsilon_{ji}|; \frac{1}{a_j + b_j M(\theta)_{ji}} \right) \\
 &= \prod_{j=1}^2 \prod_{i=1}^{N_j} \frac{1}{2(a_j + b_j M(\theta)_{ji})} \exp \left( \frac{-|\varepsilon_{ji}|}{a_j + b_j M(\theta)_{ji}} \right), \quad (4)
 \end{aligned}$$

where  $\mathbf{Y}$  represents the observations,  $\theta$  the parameters of the PRELES model,  $M(\theta)$  the outputs of model,  $\varepsilon$  the measurement error and an unknown model structural error.  $\text{Exp}(\cdot; \cdot)$  is the probability density function of the exponential distribution, and  $\frac{1}{a_j + b_j M(\theta)_{ji}}$

is its rate parameter. The  $j$ -subscripts index the two types of output variable, which are GPP and ET; the  $i$ -subscripts index the data and  $N_j$  is the total number of valid observations for variable  $j$ . Parameters  $a$  and  $b$  were calibrated simultaneously with  $\theta$  to approximate the relationship between rate parameter and measurement uncertainty.

For each forest-climate cluster, we proposed a generic vector of parameters by multisite calibration within a Bayesian hierarchical modelling approach (Figure S8, Section S5). For each PFT (Table 2), data from different sites were combined in BC. The sites within one PFT shared the same generic parameters, which means eventually nine vectors of generic parameters were

obtained respectively for the nine PFTs. To explain the variation within one PFT, two parameters, potential LUE ( $\beta$ ) and measurement uncertainty intercept ( $a$ ), were considered 'site-specific' and generated from distributions that represented random effects. Then the joint posterior distribution of parameters  $p(\theta|\mathbf{Y})$  is written as follows:

$$\begin{aligned}
 p(\theta, c, d, g, h|\mathbf{Y}) &\propto \prod_{j=1}^2 \prod_{s=1}^S \prod_{i=1}^{N_{js}} \text{Exp} \left( |\varepsilon_{j,s,i}|; \frac{1}{a_j + b_{js} M(\theta)_{j,s,i}} \right) \\
 &\times \prod_{j=1}^2 \prod_{s=1}^S \Gamma(a_{js}; c_j, d_j) \prod_{s=1}^S \Gamma(\beta_s; g, h), \quad (5)
 \end{aligned}$$

where the  $s$ -subscripts index the site and  $S$  is the total number of sites in one cluster,  $\Gamma(\cdot; \cdot)$  represents the probability density function of the gamma distribution that describes the heterogeneity of potential LUE and measurement uncertainty,  $c$  and  $g$  are the shape parameters of the gamma distributions, and  $d$  and  $h$  are the rate parameters. The gamma distribution was chosen because we assumed that  $\beta$  and  $a$  were nonnegative and followed right-skewed distributions, based on the results of site-specific calibrations. The priors and hyperpriors were ignored in Equation (5) because they were assumed as independent uniform distributions. The ranges of uniform distributions for parameters in PRELES were given in Table 1. Detailed explanations for the structural distinctions of site-specific calibration and multisite calibration are given in Section S5.

### 2.3.3 | MCMC sampler and convergence diagnostic

Markov chain Monte Carlo (MCMC) sampling techniques were used (Hastings, 1970; Metropolis, Rosenbluth, Rosenbluth, Teller, & Teller, 1953) since the posterior distribution was nonanalytical.

The MCMC was simulated, using differential evolution adaptive Metropolis with snooker updating (DREAMzs), which runs a few chains in parallel and explores the parameter space in an efficient way (Laloy & Vrugt, 2012; Vrugt et al., 2009). We used the DREAMzs algorithm implemented in the R package BayesianTools (Hartig, Minunno, & Paul, 2017).

The MCMC convergence diagnostic (Brooks & Gelman, 1998; Gelman & Rubin, 1992) was used to monitor the convergence in the MCMC output. The multivariate potential scale reduction factor (MPSRF) was calculated, based on two MCMC runs, each of which has three internal chains. A large MPSRF means that the output from all chains is distinguishable and a notable difference exists between variance and intrachain variance. In our study, convergence was diagnosed when the MPSRF was below 1.05, which is a relatively strict criterion (Brooks & Gelman, 1998).

### 2.3.4 | Model evaluation

Model performance was evaluated using a systematically designed cross-validation procedure. Calibration strategies were designed separately for six different cases of applying PRELES at a given site:

1. S-S: Data from a site are available for model calibration. This leads to *site-specific calibration*.
2. M-S: Data from the subject site and from other sites in the same PFT are available for calibration. This yields *multisite calibration*.
3. S.in: No data are available for the subject site. Predictions are made with and S-S calibration of another site in the same PFT.
4. M.in: No data are available for the subject site. Predictions are made with and M-S calibration of other sites in the same PFT.
5. S.out: No data are available for the subject site. Predictions are made with and S-S calibration of a site in a different PFT.
6. M.out: No data are available for the subject site. Predictions are made with and M-S calibration of other sites in a different PFT.

A twofold validation strategy was applied to calculate the model-data mismatches. For each time, half of the GPP and ET observations from the site were randomly selected for the model calibration, and the remaining observations were used for the validation. In cases (3)–(6), the data from the subject site were excluded in calibration but was used for validation. Eventually, the reliability and stability of both the PRELES model and calibration strategies were evaluated for each site independently. A comparison of cases (1) and (2) informed us about the applicability of a generic parameter vector of the PFT. Cases (3)–(6) were designed to find out what calibration strategy to adopt when applying PRELES

to new sites without any flux data or LUE-related information. Additionally, the model reliability in the extrapolation during the drought event in 2018 was assessed using another eddy covariance data set 'Drought 2018' (Drought 2018 Team & ICOS Ecosystem Thematic Centre, 2019) and MODIS GPP product MOD17A2H (Running, Mu, & Zhao, 2015; ORNL DAAC, 2018) in Section S6.

Besides the root mean squared error (RMSE), we also used the partitioning of the mean squared error (MSE) that provides both statistical and graphical analysis for model performance (Theil, 1966). Kobayashi and Salam (2000) demonstrated that the MSE could be divided into three components by comparing the measurements and predictions: squared bias (SB), squared difference between standard deviations and lack of correlation (LC) weighted by the standard deviation. Gauch, Hwang, and Fick (2003) suggested a slightly different partitioning of MSE: SB, nonunity (NU) slope and LC. These three MSE components are distinct and additive and relate transparently to correlation and linear regression parameters. The quality and difference of these approaches were commented on in an exchange of letters by the authors (Gauch, Hwang, & Fick, 2004; Kobayashi, 2004). Here, we adopted Gauch's method, and the statistics were calculated as follows:

$$MSE = \frac{\sum_{i=1}^n (X_n - Y_n)^2}{N} = SB + NU + LC, \quad (6)$$

$$SB = (\bar{X} - \bar{Y})^2, \quad (7)$$

$$NU = (1 - s)^2 \left( \sum \frac{(X_n - \bar{X})^2}{N} \right), \quad (8)$$

$$LC = (1 - r^2) \left( \sum \frac{(Y_n - \bar{Y})^2}{N} \right), \quad (9)$$

where  $\bar{X}$  and  $\bar{Y}$  are, respectively, the means of the model predictions ( $X$ ) and observations ( $Y$ );  $s$  is the slope of the least-squares regression of  $Y$  on  $X$ ;  $r^2$  the square of the correlation coefficient and  $N$  the number of observations. SB represents the translation, which is the mean squared distance between the simulations and measurements. NU represents the rotation away from the 1:1 line of equality and LC the scatter that practically represents the random errors. In other words, SB represents the annual overestimation or underestimation of PRELES; NU shows whether the model is equally reliable in both low and high predictions; and LC is the random error that was not considered or explained in PRELES.

## 3 | RESULTS

### 3.1 | PFT differences in the posteriori parameters

The posterior of the parameters differed with the sites or PFTs (Figure 2). Distinctions between the PFTs were revealed by comparisons of the multisite calibrations. The tropical EBFs (EBF-Am) showed the highest evaporation parameter  $\chi$  and transpiration parameter  $\alpha$ . Except for the tropical cluster, DBFs needed higher temperatures to

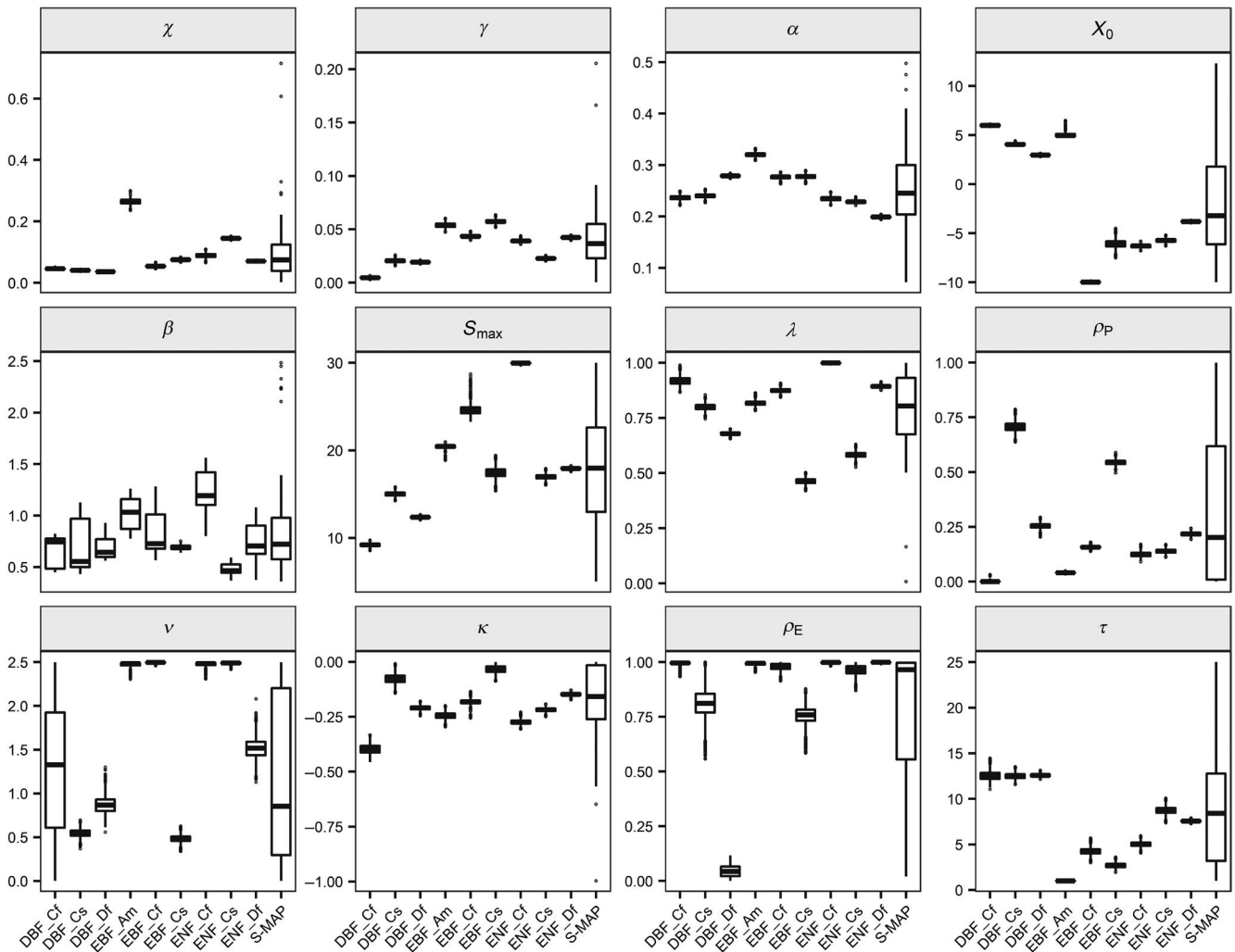


**FIGURE 2** Marginal posterior distribution of parameters for multisite calibrations of nine plant functional types (Table 2) and the summary of maximum a posteriori parameter vectors of the site-specific calibrations (S-MAP). DBF, deciduous broad-leaved forest; EBF, evergreen broad-leaved forest; ENF, evergreen needle-leaved forest; MAP, maximum a posteriori probability estimate

start the temperature acclimation (higher  $X_0$ ) than evergreen forests. The delay parameters for the ambient temperature response ( $\tau$ ) in deciduous forests were longer than in evergreen forests. The EBFs were more strongly affected by light saturation (higher  $\gamma$ ) than DBFs.

Distinctions of parameters between the PFTs could also be shown in site-specific calibrations once the parameter correlations were considered (Figure 3). The correlations resulted from the mutual effects of the parameters and partially compensated for the distinctions between sites. Although the correlations differed among the sites, a general pattern was found in the 55 site-specific calibrations (Figure S7). The highest parameter correlation was between the potential LUE ( $\beta$ ) and the light saturation parameter ( $\gamma$ ). The second highest correlation occurred between two parameters in the temperature modifier, which were the beginning ( $X_0$ ) and the maximum ( $S_{\max}$ ) of the acclimation state. Moreover, the third pair comprised the transpiration coefficient ( $\alpha$ ) and evaporation coefficient ( $\chi$ ). The correlations of the parameters occurred not only in the posterior distributions for each site-specific calibration, but also on a global scale. A strongly negative correlation ( $r_{\text{Pearson}} = -.6$ ) was found between two threshold parameters,  $X_0$  and

$S_{\max}$ , by summarizing the calibrations of various sites (Figure 3a). The DBFs acquired higher  $X_0$  than did the ENFs. The uncertainty in the parameters greatly differed among the sites. Another distinction between forest types was revealed by parameters  $\beta$  and  $\gamma$  (Figure 3b). The EBFs acquired higher  $\gamma$  than did the DBFs. The sites with larger  $\beta$  also contained higher levels of uncertainty, for example AU-Rob and AU-Wac. The distinctions of temperature acclimation between forest types were not only revealed by the parameters, but also by the temperature modifier (Figure 4). The mean values of  $f_5$  for boreal ENF sites were about 0.4, whereas for the EBFs of tropical sites the values were around 0.9. DBFs showed lower  $f_5$  than evergreen forests, even with the same mean annual temperature.

### 3.2 | Site-specific calibration versus multisite calibration

The ranges of the parameters varied widely between sites in the site-specific calibration (S-MAP in Figure 2), whereas the multisite



**FIGURE 3** (a) Thresholds of start ( $X_0$ ) and maximum ( $S_{max}$ ) of the temperature acclimation modifier. (b) Potential light-use efficiency ( $\beta$ ) and light saturation parameter ( $\gamma$ ) of the light modifier. The range bars represent the uncertainty in the parameters, which is a 95% Bayesian credible interval. The dashed lines are from linear regressions. DBF, deciduous broad-leaved forest; ENF, evergreen needle-leaved forest; EBF, evergreen broad-leaved forest;  $f_{APAR}$ , fraction of absorbed photosynthetically active radiation

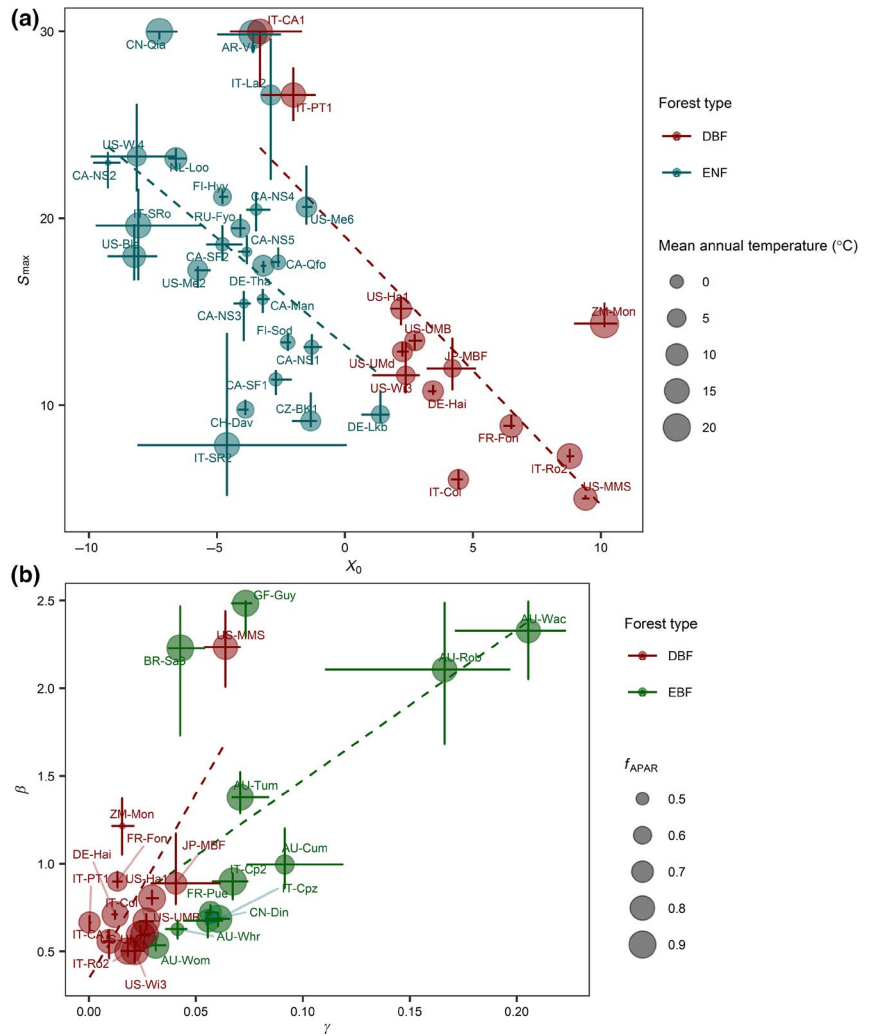
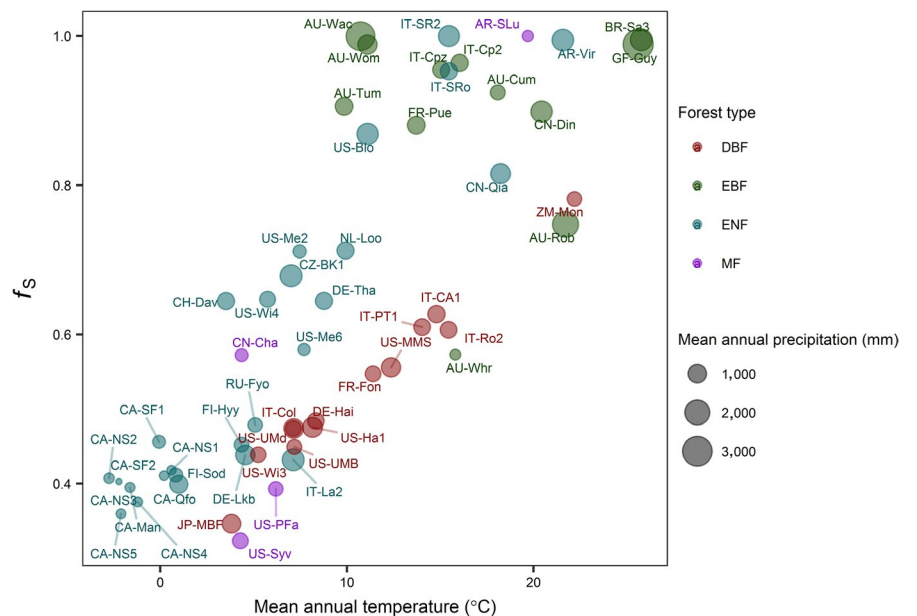


**FIGURE 4** Mean annual value of temperature acclimation modifier for various forest types. DBF, deciduous broad-leaved forest; EBF, evergreen broad-leaved forest; ENF, evergreen needle-leaved forest; MF, mixed forest. The  $f_s$  is a modifier that accounts for temperature acclimation (in Equation 1)



calibration strictly constrained the ranges of the parameters. In comparison to the observations, the calibrated PRELES model effectively simulated the seasonal variations within sites for most

PFTs (Figure 5). This means that different parameter vectors can lead to the similar model performance. By adding measurement errors that consider residual distributions, the predictive

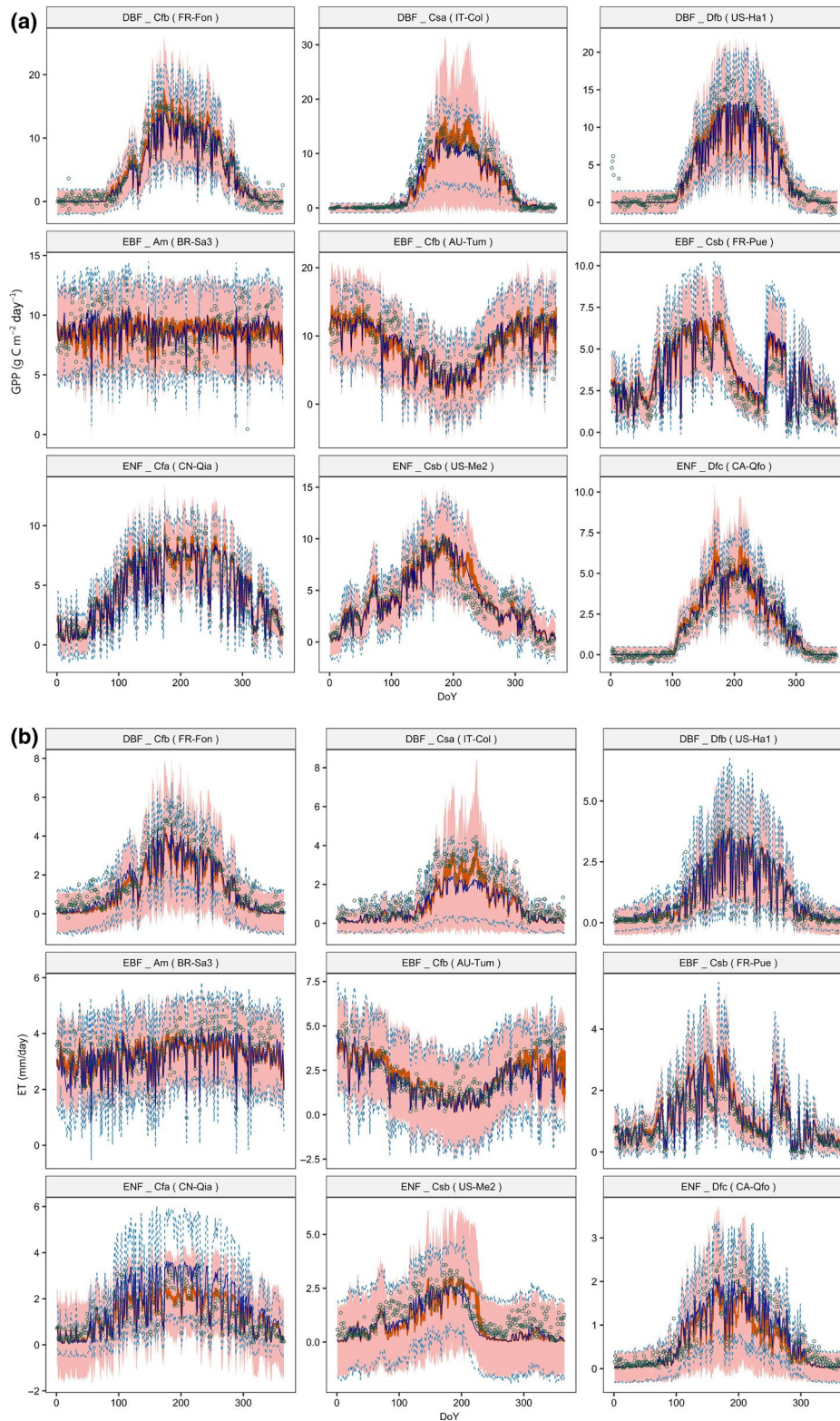


**FIGURE 5** (a) Daily gross primary production (GPP) and (b) daily evapotranspiration (ET) for nine plant functional types (PFTs). One site and 1 year were randomly selected from each PFT. The circles represent observations of eddy covariance measurements. The orange areas represent the uncertainty in the multisite calibrated model in the case M-S (Section 2.3.4). The dark orange area is the parametric uncertainty. The light orange area represents the predictive uncertainty given by the parametric uncertainty and measurement error. The dark blue solid line is generated by site-specific calibrations with MAP (maximum a posteriori parameter vector) in the case S-S. The dashed lines represent the ranges of predictive uncertainty based on the site-specific calibration. DBF, deciduous broad-leaved forest; DoY, day of year; EBF, evergreen broad-leaved forest; ENF, evergreen needle-leaved forest

uncertainty describes the ranges of eddy covariance observations that could possibly occur. For the two Mediterranean climate clusters, the declines in GPP and ET during the dry summer were captured in model simulations. The prediction uncertainty also covered the variation in daily measurements. It was difficult to judge the tropical sites, since there was no seasonal pattern, and the main environmental driver for the daily variation was unclear. Even though precipitation seems to relate with the daily GPP, the Pearson correlation was always lower than 0.2 on both weekly and monthly steps. Models based on multisite calibration and site-specific calibration performed similarly in the simulations of both GPP (Figure 5a) and ET (Figure 5b). Distinctions only occurred occasionally in a few site-year cases, and it was difficult to judge which calibration was better based on observations, because one fitted the higher observations and the other the lower observations (e.g. IT-Col in Figure 5a, CN-Qia in Figure 5b).

The accuracy of the predictions varied markedly among the sites (Figure 6). For the average model–data mismatches in multisite calibration, the proportion of random error (LC) in the MSE of GPP was 93%. For the mismatch in seasonal variation (NU) and mean bias of annual prediction (SB), the proportions were 3% and 4% respectively. The accuracy of the ET predictions was lower, since 17% of the MSE was SB, and for most sites the ET biases were due to underestimation. The main component of the deviation was LC for both site-specific and multisite calibrations. In comparison to MSE with site-specific calibrations, multisite calibrations showed 12% higher MSE for GPP and 14% higher for ET on average. The accuracy differences between site-specific and multisite calibrations were generally negligible, but noticeable for a few sites (Figure 6).

Although the multisite calibrations showed higher model–data mismatches, they could be more reliable in certain cases, especially for site-years with inadequate data (Figure 7). The MSE of multisite calibration for site-year IT-Cpz\_2001 was 13% higher than that of

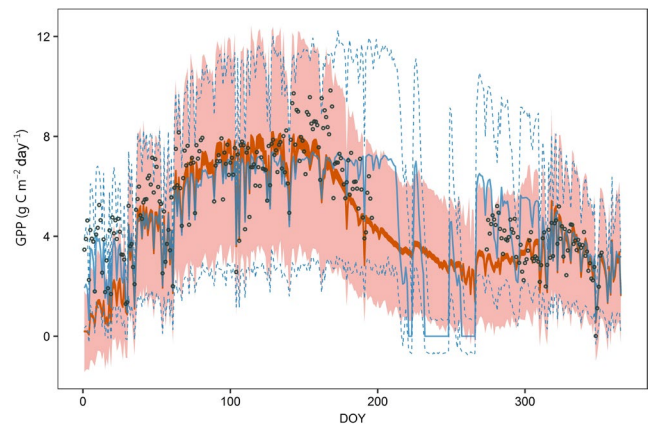
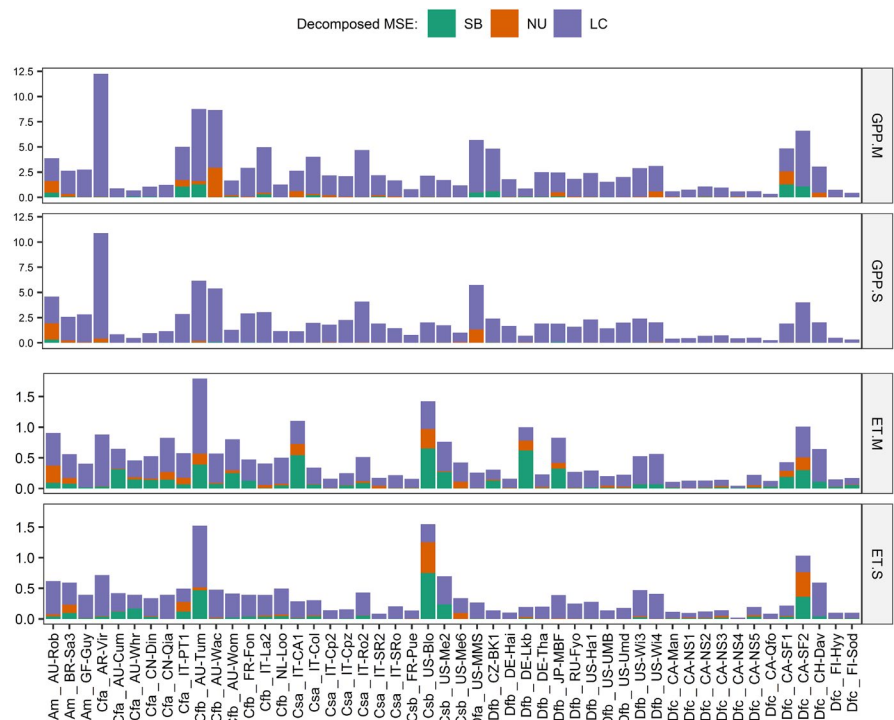


**FIGURE 7** Comparison of site-specific calibration and multisite calibration for the site with inadequate data (site-year: IT-Cpz\_2001; Table S1). The orange areas represent the uncertainty in the multisite calibrated model in the case M-S (Section 2.3.4). The dark orange area is the parametric uncertainty. The light orange area represents the predictive uncertainty given by the parametric uncertainty and measurement error. The blue solid line is generated by site-specific calibrations with MAP (maximum a posteriori parameter vector) in the case S-S. The dashed lines represent the ranges of predictive uncertainty based on the site-specific calibration. DOY, day of year; GPP, gross primary production

**FIGURE 6** Decomposed mean squared error (MSE) for prediction of gross primary production (GPP,  $\text{g C m}^{-2} \text{ day}^{-1}$ ) and evapotranspiration (ET, mm/day) based on site-specific calibrations (S) in the case S-S (Section 2.3.4) and multisite calibrations (M) in the case M-S. LC, lack of correlation; NU, nonunity; SB, squared bias



the site-specific calibration. Only 20% of daily flux observations was deleted based on the data quality during 6 years. However, for the data gap during the dry season in 2001, the site-specific calibration described the daily GPP as oscillating unrealistically, whereas the multisite calibration showed a reasonable pattern of decreasing productivity.

### 3.3 | Extrapolations and site random effects

PREdict Light-use efficiency, Evapotranspiration and Soil water integrates simplified ecosystem processes associated with GPP and ET. However, the reliability of extrapolation beyond the ranges of

calibration data sets depends on how different the plant traits and environment conditions have been changed. To evaluate our estimates of GPP and ET, four kinds of parameter vectors representing cases (3)–(6) were calculated (Figure 8). The S-S calibration provided a baseline for this. In the out-of-sample testing, S.out shows the highest risks in the extrapolations, while the M.out calibrations were more reliable. For the EBF\_Cs and EBF\_Am forests, using data from the same PFT in calibration could distinctly reduce the errors in extrapolation.

The mean of a gamma distribution  $\Gamma(\beta; g, h)$  in Equation (5) was adopted as the value of  $\beta$  in the evaluation when multisite calibration was used because the tree species and site fertility were assumed unknown for the new sites. For each PFT, this value was calculated

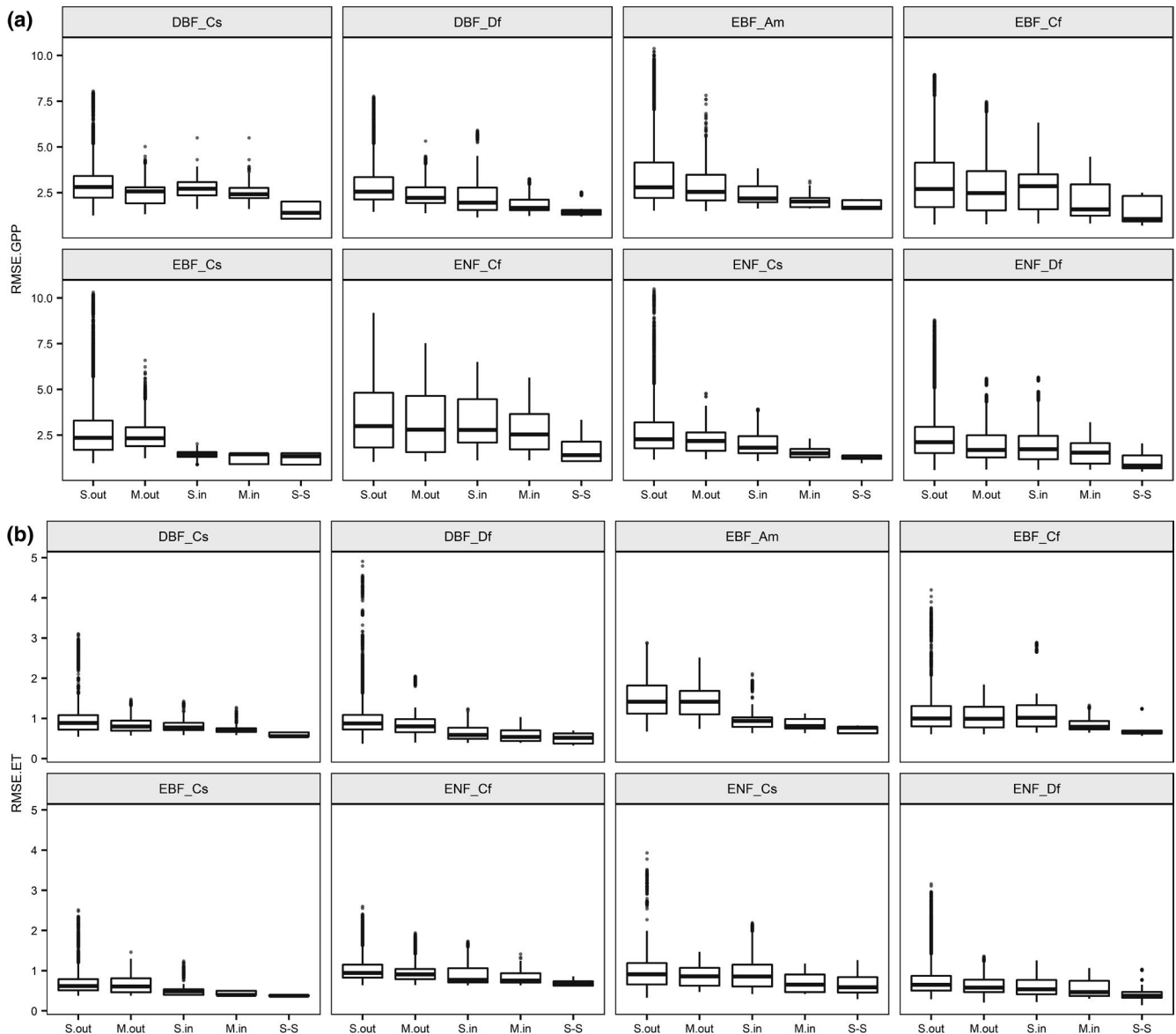


**FIGURE 8** Root-mean-squared error (RMSE) of daily (a) gross primary production (GPP,  $\text{g C m}^{-2} \text{ day}^{-1}$ ) and (b) evapotranspiration (ET) in the out-of-sample testing. The RMSE values were grouped based on the plant functional type (PFT) of validation sites. S.out, site-specific calibration of sites from other PFTs; M.out, multisite calibration of other PFTs; S.in, site-specific calibration of other sites in same PFT; M.in, multisite calibration of the same PFT but excluding data from the validation site; S-S, interpolations while using half of data for calibration and other half for validation

as  $g/h$  in Equation (5). The performance of PRELES in the case M.in can be largely improved by only adjusting the parameter  $\beta$  (Figure 9). The performance of cluster EBF\_Cs was distinctively better than the others in the validation, because all three sites represented the same tree species (*Quercus ilex*; Table S1).

Compared with the extrapolation within one PFT, the extrapolation beyond the PFT might lead to a higher risk. The site CN-Cha, which is a MF with dry springs, was not included in any cluster of the multisite calibrations. The composition of tree species makes this site neither ENF nor DBF, and the climate of this site could be classified as either Df or Dw (Table 1). We simulated the GPP and ET of this site, using parameters respectively calibrated from the two spatially closest sites (CN-Qia and JP-MBF, Figure 1) and two climate-similar PFTs (ENF-Df and DBF-Df). The simulation from the CN-Cha site-specific calibration accurately matched the observations, because it was originally calibrated with data from this site, while the simulations from the other four calibrations showed biases

and a large degree of uncertainty (Figure 10). The CN-Qia version of the calibration failed to simulate the spring GPP of the colder site CN-Cha, because their temperature acclimation processes were very different (Table S1). Meanwhile, the evaporation was highly overestimated in spring. The JP-MBF site was similar to the CN-Cha site for coldness, but was more humid with higher precipitation, which made the JP-MBF version fail in the simulation of the late spring drought at the CN-Cha site. In comparison to the site-specific versions, the two multisite calibrations performed better in both GPP and ET simulations. The higher prediction uncertainty covered the variations more thoroughly in the GPP simulations and more efficiently in the ET simulations. Nevertheless, the random effect of  $\beta$  introduced a large degree of parametric uncertainty into the simulations. For the DBF-Df in Figure 10, on average 16% of the predictive uncertainty of GPP and 13% of the uncertainty in ET were due to parametric uncertainty. For site-specific calibrations, the average proportions of parametric uncertainty were only about 5% (Figure S1).

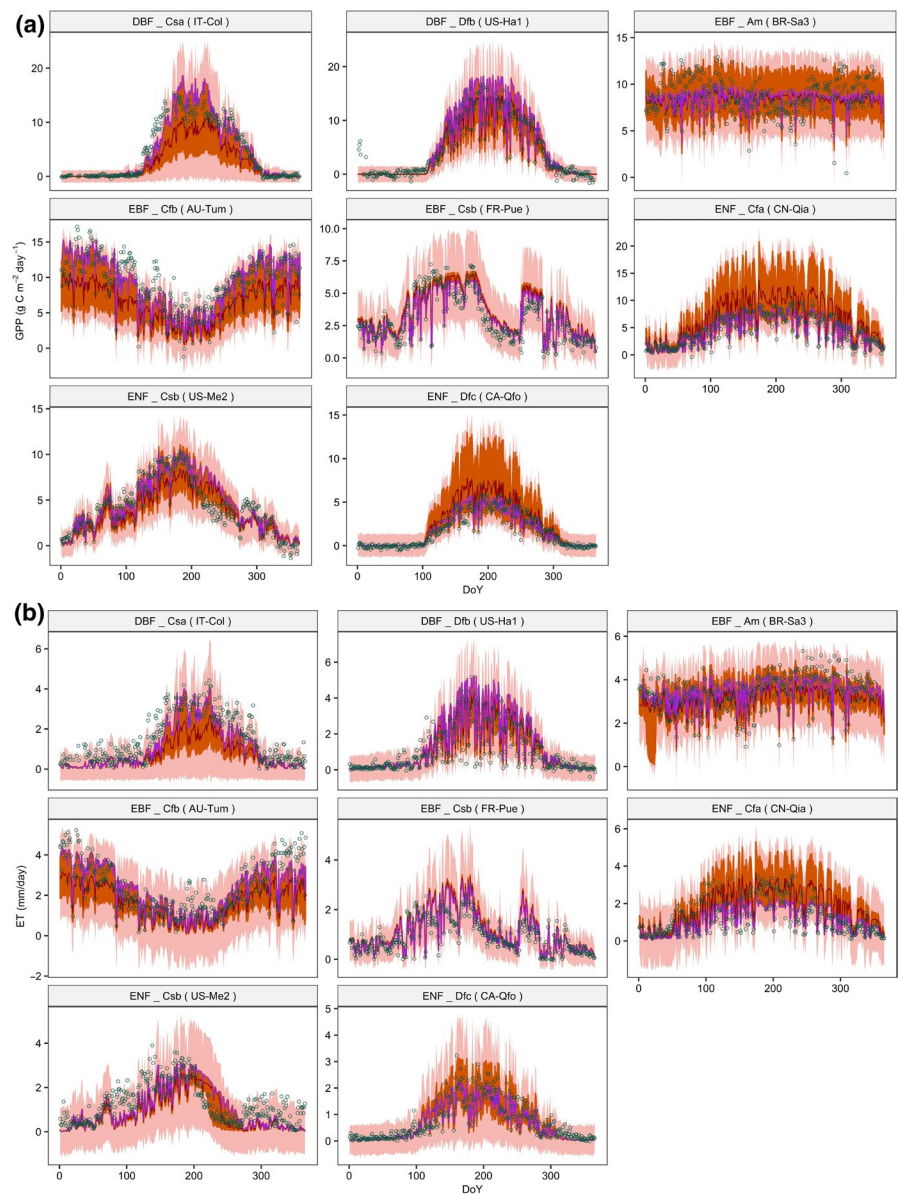


**FIGURE 9** (a) Daily gross primary production (GPP) and (b) daily evapotranspiration (ET) for nine plant functional types (PFTs). One site and 1 year were randomly selected from each PFT. The circles represent observations of eddy covariance measurements. The orange areas represent the uncertainty in the multisite calibrated model (case M.in). The dark orange area is the parametric uncertainty. The light orange area represents the predictive uncertainty given by the parametric uncertainty and measurement error. The red solid line is generated by the MAP (maximum a posteriori parameter vector) in the case M.in while using the mean of the parameter  $\beta$  in the cluster (calculated as  $g/h$  in Equation 5). The purple solid line is generated by the MAP in the case M.in while adjusting the parameter  $\beta$  using fluxes data in the validation site. DBF, deciduous broad-leaved forest; DoY, day of year; EBF, evergreen broad-leaved forest; ENF, evergreen needle-leaved forest

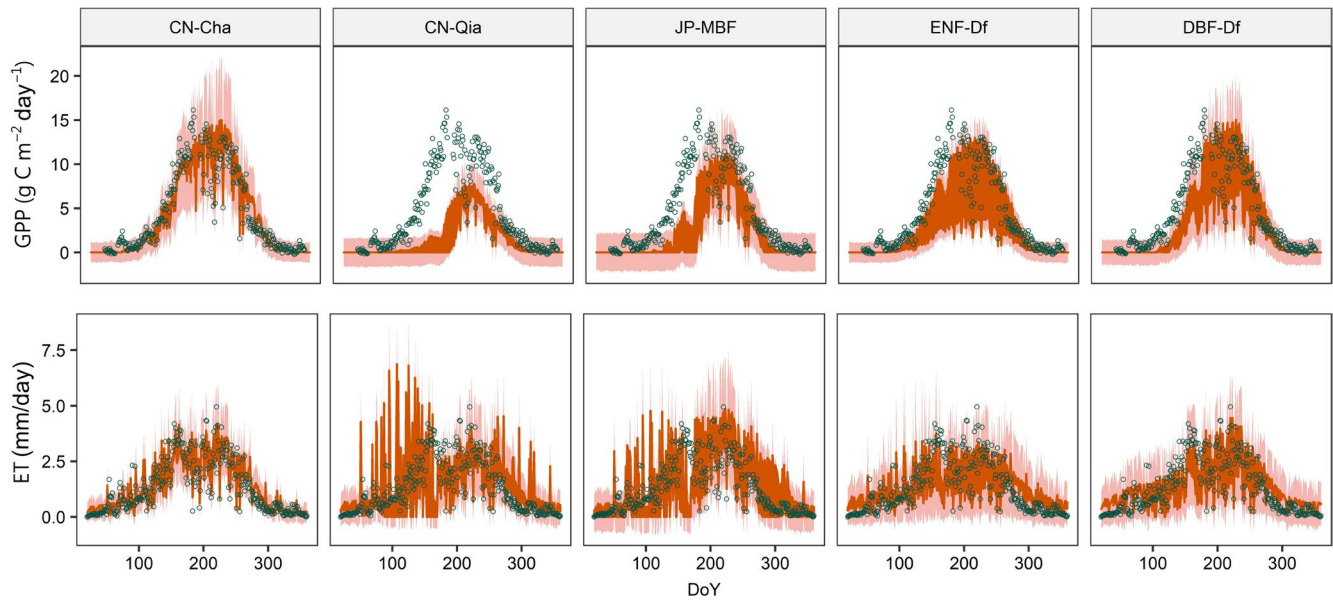


**FIGURE 10** Validation of different calibrations of PRELES with observations at the dry spring site CN-Cha. The circles represent observations of eddy covariance measurements at site CN-Cha. The orange areas are model simulations based on calibrations from different sites. The dark orange area is the parametric uncertainty. The light orange area represents the predictive uncertainty given by the parametric uncertainty and measurement error. DoY, day of year; ET, evapotranspiration; GPP, gross primary production; PRELES, Predict Light-use efficiency, Evapotranspiration and Soil water

## 4 | DISCUSSION

The model calibrations and validations demonstrated that PRELES could accurately simulate GPP and ET on a large geographical scale. The simulations were reliable even for extremely contrasting environmental conditions and distinctive forest ecosystems when given sufficient data. The multisite calibrations were as accurate as the site-specific calibrations in the interpolations, but were more reliable in the extrapolations. Based on the hierarchical quantification of the random effects among sites, the predictive uncertainty was extensive for extrapolations to new sites with unknown tree species and site fertility.

### 4.1 | A generic parameter vector

Minunno et al. (2016) examined a generic calibration of PRELES for the boreal coniferous forests in Fennoscandia and showed that the multisite calibration and the site-specific calibration performed similarly. In this study, we extended the applications of PRELES to a larger regional/global scale, using a Bayesian hierarchical modelling approach. PRELES assumes that the actual LUE changes with weather conditions, including the intensity of light, temperature, VPD and soil water. The generality of parameters in LUE models depends on the complexity of model structures and the accuracy of input data. On the one hand, a universal set of parameters can be sufficient enough for satellite-driven LUE models across biomes and geographic regions (Yuan, Cai, Liu, et al., 2014). On the other hand, various studies have illustrated that

many other external factors also affect the LUE, including age of trees (Saldarriaga & Luxmoore, 1991), fertilization treatment (Leuning, Cromer, & Rance, 1991), specific leaf nitrogen (Hammer & Wright, 1994; Kergoat, Lafont, Arneth, Le Dantec, & Saugier, 2008; Peltoniemi et al., 2012) and tree species (Ahl et al., 2004). Since these factors were not considered in the calibrations when combining the data, we assumed that the potential LUE  $\beta$  was different among sites (Figure S8). Thus, the crucial assumption became that the differences among sites within a single cluster could be simulated by simply adjusting the potential LUE, which was confirmed and illustrated in Figure 9 and Figure S10. The performance of the site-specific and multisite calibrations was similar (Figure 5), and the differences between them in the Decomposed MSE tests (Figure 6) were almost negligible, which also corroborated this assumption.

The site-specific calibration assumes that the sites are completely unrelated. The boreal-region generic calibration in the study of Minunno et al. (2016) ignored all site-to-site variability. The challenge in our global data analysis and forecasting is to correctly partition different sources of variability. Our multisite calibration represents the continuum between treating data sets independent versus treating them identical. As a result, we partitioned process variability between the different levels of the hierarchy (Section S5). Using a Bayesian hierarchical modelling approach, the random effect among sites was quantified not only for the potential LUE  $\beta$  but also for the measurement uncertainty parameter  $a$  (Equation 5; Figure S8). The intercept  $a$  was chosen, due to its wider range of variation compared with the slope (Richardson et al., 2008). This pattern was blurred with the results of the 55 site-specific calibrations.

The intercept  $a$  varied among the sites, with values from 0.10 to 2.42 g C m<sup>-2</sup> day<sup>-1</sup> for GPP and 0.004 to 0.99 mm/day for ET. By comparison, the slope  $b$  was confined from 0.0007 to 0.36 for GPP and 0.0001 to 0.70 for ET.

The main motivations for applying the hierarchical Bayesian framework in this study include combining data sets with different measurement errors, integrating the random effects for each site and quantifying the uncertainty. The Bayesian framework consistently provided natural structures for achieving these purposes by treating all terms in the model calibrations and predictions as probability distributions (Clark, 2007; Dietze, 2017). Nevertheless, it is also possible to achieve a generic parameter vector by other mathematical methods. Combinations of multisource data could be considered as having multiple likelihoods or weighted objectives (Marler & Arora, 2010). Random effects could be characterized by multilevel mixed models (Bijleveld et al., 1998; Ware & Liang, 1996). Uncertainty quantification could be achieved by the bootstrap method (Efron, 1979).

## 4.2 | Interpolation versus extrapolation

Based on the site-specific and multisite calibrations, three different vectors of PRELES parameters were optional for applications: the site-specific calibrated version, the multisite calibrated version with a 'site-specific' LUE parameter  $\beta$  and 'site-specific' measurement uncertainty  $a$ , and the multisite calibrated version with unknown values (random effects) of  $\beta$  and  $a$ . The latter two parameter vectors were only two different strategies for using the multisite calibration. This is not to say that one of them is generally better or always more reliable than the other; instead, the choice of method is dependent on the objectives of the model used. When the analysis is based on a local scale or a region of the same site condition and a comprehensive and complete data set is available (Minunno et al., 2016), site-specific calibration would be the best option. In forestry practice, however, it is common that a data set with various possible local weather conditions is unavailable or difficult to access. Moreover, the model applications often involve a wider variability in terms of climate and forest structure. In that case, the multisite calibration with site-specific  $\beta$  and  $a$  would be more reliable than the site-specific calibration (e.g. IT-Cpz in Figure 7 and Figure S1c). When the model is extrapolated to new situations with unknown tree species and site fertility, multisite calibration of the same PFT should be the best option, and site-specific calibration of other sites in same PFT should be the next-best option (Figure 8). The choices of parameter vectors should depend on the similarity of PFTs instead of geographical distances. For instance, when we validated several calibrations for the site CN-Cha, which was not included in the multisite calibration (Figure 10), the site-specific potential LUE parameter  $\beta$  and measurement uncertainty parameter  $a$  were not available from the original calibration. Thus, we generated these two parameters from the gamma distributions calibrated in the hierarchical Bayesian modelling approach (Equation 5). The random effects in

multisite calibration reflect the actual predictive uncertainty when extrapolating entirely outside the original sites. If more information were available about  $\beta$ , possibly based on tree species and site fertility (canopy nitrogen concentration), we could also have decreased the uncertainty by constraining the value of  $\beta$  (the purple lines in Figure 9 and Figure S10).

## 4.3 | The role of data quality

The input of soil information is crucial for simulations of the soil-water content. We collected the information from three global gridded data sets, which were inaccurate and may have affected the simulations of drought events. The field water capacity and wilting point are determined by the physical properties of the soil (Kirkham, 2014). Both soil texture and soil depth might vary widely with the terrain. The strong correlations between soil parameters allowed only one parameter to be adjusted. When calibrating all soil-related parameters simultaneously, the marginal posterior distribution simply converged to the prior distribution, which means that the uncertainty in this parameter was entirely dependent on the prior information (similar with the case of CO<sub>2</sub> module; Section S3). When comparing those soil data sets with field measurements (literature in Table S1), larger mismatches were found in soil depth than in soil texture. We chose to calibrate only the soil depth for each site in the site-specific calibration by using the information from global data sets as the prior. Eventually, the adjustments improved the simulations of those sites with drought events or dry seasons.

The  $f_{\text{APAR}}$  is another important input for PRELES, and it interfered with the estimation of  $\beta$  in the calibrations. We exercised particular care in interpreting the  $f_{\text{APAR}}$  data. We filtered the  $f_{\text{APAR}}$  data and fitted the harmonic model, using only the observations during the growing seasons. Even so, large random errors and biases could still be contained in the simulated curves of  $f_{\text{APAR}}$  (Figure S2). Although it was theoretically possible to compare the maximum LUEs of all the different tree species after calibration, the error propagated from  $f_{\text{APAR}}$  obscured any relevant interpretations.

The global scale evaluation of the model is dependent not only on the applicability of the model itself but also on the quantity and quality of the data. We filtered the eddy covariance data, based on the quality flag, but outliers still occurred, which widened the mismatches. For sites with few quality-acceptable observations, the outliers resulted in higher NU or SB (e.g. ET performance of site CA-SF2). The outliers were one of the main reasons that residuals followed double-exponential distributions instead of normal distributions. The heavy-tailed distributions likely weakened the impact of erratic observations and outliers (Sivia & Skilling, 2006). The differences between the S-S and M-S calibrations in model-data mismatch were imperceptible (Figure 6), but the real performance could differ noticeably between the calibrations for certain gap periods (e.g. the dry season of IT-Cpz and the spring of US-Wi3 in Figure S1c). This suggests that the information lost in gaps could have been useful for the calibrations.

Considering that most sites in our study were from boreal and temperate forests in Europe and North America, extrapolation to forests of Asia, South America and Africa could be problematic, especially for the tropical forests. No seasonal or monsoon pattern was revealed by PRELES for the tropical sites (Figure S1a). Gebremichael and Barros (2006) found that the MODIS GPP products showed large degrees of uncertainty and were biased in the tropical monsoon regions when validated with flux tower observations. Yuan, Cai, Xia, et al. (2014) compared seven LUE models on a global scale and illustrated that most models performed better in capturing the temporal changes and magnitude of GPP in DBFs and MFs than in the EBFs. Although the model–data mismatch increased with mean annual temperature (Figure S5), it is still difficult to interpret which PFT was not suitable for PRELES. For example, the site GF-Guy showed the highest model–data mismatch for predicting GPP (Figure 6), which was actually caused by its extremely high tree species richness and productivity (Bonal et al., 2008). The measurement errors, stand structure and silviculture treatments varied immensely within single PFTs, which obscured the distinctions among PFTs.

#### 4.4 | Biological interpretation of parameters

Instead of using direct physiological measurements of the parameters, this study applied BC and eddy covariance data to adjusting parameter values at the level of the whole system. One common concern about this approach is whether the parameters still have a biological meaning. An inadequate data set may lead to overfitting (e.g. outliers of MAPs in site-specific calibrations in Figure 2). Since the inverse modelling approach to model calibration is based on statistical analysis instead of detailed physiological measurements, the MAPs may easily have deviated from physiologically meaningful parameter values if the uncertainty ranges were not efficiently constrained by the data. Similarly, the correlations between parameters may have led to wide uncertainty ranges (e.g. IT-SR2 in Figure 3a). In these cases, different combinations of parameters could have led to the same predictions, implying that the data used in the calibration were not sufficient to reduce the parametric uncertainty. A data set from tropical or subtropical sites may not effectively constrain the parameters of the temperature modifier, which was the reason for setting the priors of  $S_{\max}$  and  $X_0$  respectively for each site or PFT based on the local temperature ranges (Table 1). The multisite calibration resulted in more accurate estimations of parameters with a lower probability of overfitting by assimilating information from a wider range of weather conditions (Figure 2). With almost the same performance, the multisite calibration contained less parametric uncertainty with more reasonable MAPs. However, the risk in multisite calibrations lies in assuming that forests from different sites respond to environmental factors in exactly the same pattern. Thus, instead of one global calibration, we adopted nine multisite calibrations respectively designed for nine PFTs.

The parameters in the temperature acclimation modifier were closely associated with the phenology of the growing season, and

plausible parameters were obtained for each PFT. In comparison to evergreen coniferous forests, deciduous forests need higher temperature for acclimation ( $X_0$ ) and longer delays for ambient temperature response, which shows that deciduous trees recover more slowly with the rising temperatures. The delay parameter for ambient temperature response  $\tau$  in the DBFs was also larger than those of other clusters (Figure 2). This distinction in spring phenology was closely linked with the adaptive strategies of DBFs and ENFs. To maximize the carbon fixation, it would benefit the DBFs to leaf-out as early as possible in spring. However, the potential risk is damage to the leaves and conducting tissues when a late frost occurs (Bennie, Kubin, Wiltshire, Huntley, & Baxter, 2010). ENFs adopt a resource-conserving strategy to produce well-defended needles that have a long lifespan, while DBFs adopt a resource-demanding strategy to produce less costly and poorly defended broad leaves (Rahman & Tsukamoto, 2013). Although the leaf-out day in spring was delayed, the DBFs actually had a longer effective growing season lengths, due to the higher recovery speed and delayed recession day of the growing season (Niu, Fu, Gu, & Luo, 2013).

The distinctions of the parameters among the PFTs were affected by both the physiological characteristics of the plants and the climate patterns. The higher value of light saturation parameter  $\gamma$  in the EBFs (Figure 3b) indicates that larger proportions of intercepted light were not utilized, due to light saturation in comparison to DBFs. This was probably due to EBFs occurring in tropical or subtropical regions, where the light intensity is much higher than that of temperate or boreal regions. Photosynthesis keeps the light saturated for longer durations in low-latitude regions, due to high irradiance, even though low-latitude plants attain photosynthetic light saturation at higher light intensity (Mooney & Billings, 1961). Extremely high light intensity may result in a decline in photosynthesis, due to photo-oxidation of photosynthetic enzymes and pigments (Lambers, Chapin, & Pons, 2008). High levels of light also lead to an increase in leaf temperature or even heat stress. Since the temperature modifier in PRELES only focuses on seasonal acclimation, the negative impacts of unfavourably high temperature are actually explained by the light saturation modifier and VPD modifier. PRELES assumes a homogeneous environment of PPFD and canopy structure to obtain the photosynthesis of the entire ecosystem, which avoids complex structures for modelling the effect of canopy positions (Campbell, Marini, & Birch, 1992) or optimal canopy nitrogen allocation (Badeck, 1995; Field, 1983).

The ET model (Equation 2) partitions the water fluxes of ecosystems into transpiration and evaporation. These two components were not sharply distinguished in the calibrations, since only total water fluxes were given in the eddy covariance measurements. Thus, higher uncertainty occurred for the ET parameters  $\nu$  and  $\rho_E$  (Figure 2). Meanwhile, high correlations occurred between transpiration parameter  $\alpha$  and evaporation parameter  $\chi$  (Figure S7). The threshold for the effect of soil-water stress on evaporation,  $\rho_{E1}$ , was distinctively low for the cluster DBF-Df (Figure 2). This may have resulted from high precipitation but low potential evaporation of its climate. In addition, the increased  $f_{\text{APAR}}$  greatly reduced the evaporation,



which made the impact of soil water on evaporation negligible at the beginning of the growing season. Most parameters in PRELES are difficult to obtain in physiological measurements. Parameter  $\lambda$  indicates the sensitivity of water use efficiency, so the range was defined as 0–1 (Table 1). However, some of the lumped-parameters are even difficult to define the prior. The parameter  $\nu$  is related to the sensitivity of water use efficiency to the rooting pattern, and its possible range was set based on pre-tests of the likelihood and convergence during calibration instead of the measurements in physiological studies.

Beer et al. (2009) found that inherent water use efficiency is higher for deciduous broad-leaved forests than evergreen needle-leaved forests based on data from 43 flux tower sites across biomes. Using MODIS and flux data at 28 sites across United States, Lu and Zhuang (2010) found that evergreen broad-leaf forest has the highest WUE, intermediate at evergreen needle-leaf forest and lowest at the deciduous needle/broad leaf forest. The parameter  $\alpha$  in PRELES was designed with a similar interpretation with the inverse of intrinsic water use efficiency (Equation 2). The posterior distribution of parameter  $\alpha$  illustrated that intrinsic water use efficiency is lowest in evergreen broad-leaved forests, especially in the tropical broad-leaved forests, but no clear distinction was found between deciduous broad-leaved forests and evergreen needle-leaved forests (Figure 2). This mismatch between PRELES parameter and previous studies might be due to incorrect partitioning among the transpiration, bare soil evaporation and water storage on canopy surface after rainy days (Grelle, Lundberg, Lindroth, Morén, & Cienciala, 1997). The parameters of the ET model might deviate from its physiologically meaningful value in order to match the observations of ecosystem total water fluxes.

#### 4.5 | Uncertainty quantification

Although many LUE models have previously been calibrated and tested against eddy covariance data (e.g. Heinsch et al., 2006; Yuan et al., 2007), the uncertainty has seldom been quantified. Zheng et al. (2018) separately analysed the uncertainty of model structure, parameters, input data and spatial resolution for remote-sensing data-based LUE models, but the contributions of various sources to the final forecasting were not qualified. Bayesian frameworks allow us to treat all terms in the forecast as probability distributions, thus making it easier to quantify uncertainty and partition uncertainties into different sources (Dietze, 2017).

The uncertainty analysis divided the predictive uncertainty into three components: parametric, measurement, and model structural uncertainty. Since only one model, PRELES, was considered in the study, the model structural uncertainty was mixed with the other two components. Measurement uncertainty, which often comprised more than 90% of the predictive uncertainty (Figure 5), represented the measurement error of GPP and ET. However, the records of GPP were not directly measured but inferred from the NEE of CO<sub>2</sub>, using partitioning algorithms (Aubinet et al., 2012). A certain amount of 'measurement uncertainty' of GPP was actually caused by the partitioning methods (Figure S4).

For predictions of GPP in climate change projections, the parametric and structural uncertainty of PRELES was almost marginal in comparison to the uncertainty propagated from emission scenarios and the global circulation model (Kallioikoski et al., 2018). However, the precondition of the low uncertainty was that a sufficient data set was obtained for the model calibration and validation in the application area that was relatively homogeneous under climate and stand conditions (Minunno et al., 2016). In the case of various forest types, the prediction uncertainty differed greatly from site to site (Figure S1). When simulations are based on extrapolation instead of interpolation, the uncertainty will be even higher (Figure 10), resulting from the assumptions of random site effects and the choice of parameters. The uncertainty for forecasting the impact of ambient CO<sub>2</sub> concentration on photosynthesis and transpirations could hardly be assessed from model calibrations (Figure S6).

#### 4.6 | Model simplifications for spatial applications

The LUE approach has been applied at various spatial and temporal scales for simulations of GPP. The spatial-scale application of process-based models is feasible, but requires spatially derived climate data, soil survey, and remotely sensed estimates of  $f_{\text{APAR}}$  (Waring et al., 2010). Model simplifications can largely reduce the data requirements and allow for simulations on a global scale. The satellite driven LUE approach has been widely used in monitoring spatial and temporal dynamics of global terrestrial GPP, relying on extensive remote-sensing data and simplified model structure. For instance, the EC-LUE model proposed by Yuan et al. (2007) was driven by four variables only: normalized difference vegetation index (NDVI), photosynthetically active radiation, air temperature and the Bowen ratio. These variables can be directly derived from remote-sensing data. Furthermore, Sims et al. (2008) developed a GPP model based solely on the enhanced vegetation index and land-surface temperature from MODIS. Methods of simplification include setting a constant biome-independent potential LUE value (e.g. Potter et al., 1993; Yuan et al., 2007), and ignoring or indirectly describing the soil-water stress (e.g. VPD accounts for drought stress in MODIS-GPP products; Running, Nemani, Glassy, & Thornton, 1999; Running et al., 2004). Zheng et al. (2018) quantified the model structure uncertainty in the LUE approach by comparing 36 combinations of optional simplified modifiers, then found the most suitable model structure for the study region. The choice of a suitable model depends on both the accuracy requirement and data availability. For instance, both MODIS GPP product MOD17A2H and PRELES captured the changes of GPP during drought events in the 2018 summer (Figure S10). The cost of accurate predictions from PRELES is the data or knowledge for unbiased estimation of parameter  $\beta$ . Otherwise, the predictions will contain large ranges of uncertainty. These satellite-based LUE models can be conveniently applied on a global scale (Yuan, Cai, Xia, et al., 2014), but the interpretations of future productivity would be problematic, especially under a changing climate. The hierarchical

modelling approach maintained the complexity of PRELES, thus avoiding the errors propagated from model oversimplification. Precipitation and soil information will be the most difficult inputs to acquire for the global simulations in PRELES, whereas other meteorological variables and  $f_{\text{APAR}}$  could be directly derived from remote-sensing products. For evergreen forests, another practical approach of estimating  $f_{\text{APAR}}$  is to use Lambert–Beer law when annual leaf area index and extinction coefficient can be obtained.

PREdict Light-use efficiency, Evapotranspiration and Soil water aims at a compromise between predictive accuracy and model complexity. The generalization of ecosystem processes on the one hand makes the model convincing in extrapolating to changing environments, and on the other hand makes it convenient to parameterize and apply on large geographical scales. The model accurately simulated and explained the seasonal and daily GPP variations for most forest-climate types. Thus, PRELES can be a good candidate for mapping forest production and quantifying uncertainty on regional to global scales under the background of climate change. The potential risk in global applications is that we only calibrated parameters, while the optimal model structure should vary as plant traits and environments change. For instance, the modifier of temperature acclimation was crucial for boreal and temperate PFTs, but was impractical for tropical forests. A key development need of PRELES for global application is to generalize and quantify the ecophysiological distinctions of varying biomes. A more reliable global calibration of PRELES should focus on not only adjusting parameters, but also optimizing the PFT-specific model structures.

#### ACKNOWLEDGEMENTS

We acknowledge the contributions of the Academy of Finland project CARB-ARC (No. 286190), the National Natural Science Foundation of China (NSFC 31640646), the Strategic Research Council at the Academy of Finland (IBC-CARBON, decision. #312635, SOMPA 312912) and the Horizon 2020 Research and Innovation Framework Program (Forest Carbon Flux and Storage Mapping Service, proposal #821860). We also appreciate English language editing by James Thompson. This work used eddy covariance data acquired and shared by the FLUXNET community, including these networks: AmeriFlux, AfriFlux, AsiaFlux, CarboAfrica, CarboEuropeIP, CarboItaly, CarboMont, ChinaFlux, Fluxnet-Canada, GreenGrass, ICOS, KoFlux, LBA, NECC, OzFlux-TERN, TCOS-Siberia and USCCC. The ERA-Interim reanalysis data were provided by the ECMWF and processed by the LSCE. The FLUXNET eddy covariance data processing and harmonization were carried out by the European Fluxes Database Cluster, AmeriFlux Management Project and Fluxdata project of FLUXNET, with the support of the CDIAC and ICOS Ecosystem Thematic Centre, and the OzFlux, ChinaFlux and AsiaFlux offices.

#### DATA AVAILABILITY STATEMENT

PREdict Light-use efficiency, Evapotranspiration and Soil water is available in C language and in an R package, and can be downloaded at <https://github.com/MikkoPeltoniemi/Rpreles/>. Calibration code

and the posterior parameter distributions of this study can be obtained on request from Xianglin Tian ([xianglin.tian@helsinki.fi](mailto:xianglin.tian@helsinki.fi)). Daily meteorological and flux records were selected and downloaded from the 'FLUXNET2015 dataset' at <https://fluxnet.fluxdata.org/> and from the 'Drought 2018' data set at ICOS Carbon Portal <https://doi.org/10.18160/PZDK-EF78>. The daily time series of  $f_{\text{APAR}}$  and MODIS GPP records throughout the growing season were collected from remotely sensed data products from the Moderate Resolution Imaging Spectroradiometer collections at [https://daac.ornl.gov/cgi-bin/dsvviewer.pl?ds\\_id=1379](https://daac.ornl.gov/cgi-bin/dsvviewer.pl?ds_id=1379). Other data that support the findings of this study are available from the authors upon request.

#### ORCID

Xianglin Tian  <https://orcid.org/0000-0001-6142-4673>

Francesco Minunno  <https://orcid.org/0000-0002-7658-6402>

Tianjian Cao  <https://orcid.org/0000-0001-5906-308X>

Mikko Peltoniemi  <https://orcid.org/0000-0003-2028-6969>

Tuomo Kallikokki  <https://orcid.org/0000-0001-8787-1279>

Annikki Mäkelä  <https://orcid.org/0000-0001-9633-7350>

#### REFERENCES

- Aber, J. D., & Federer, C. A. (1992). A generalized, lumped-parameter model of photosynthesis, evapotranspiration and net primary production in temperate and boreal forest ecosystems. *Oecologia*, 92(4), 463–474. <https://doi.org/10.1007/bf00317837>
- Ahl, D. E., Gower, S. T., Mackay, D. S., Burrows, S. N., Norman, J. M., & Diak, G. R. (2004). Heterogeneity of light use efficiency in a northern Wisconsin forest: Implications for modeling net primary production with remote sensing. *Remote Sensing of Environment*, 93, 168–178. <https://doi.org/10.1016/j.rse.2004.07.003>
- Aubinet, M., Vesala, T., & Papale, D. (2012). *Eddy covariance: A practical guide to measurement and data analysis*. Germany: Springer Science & Business Media. Retrieved from <https://doi.org/10.1007/978-94-007-2351-1>
- Badeck, F. (1995). Intra-leaf gradient of assimilation rate and optimal allocation of canopy nitrogen: A model on the implications of the use of homogeneous assimilation functions. *Functional Plant Biology*, 22, 425–439. <https://doi.org/10.1071/pp9950425>
- Beer, C., Ciais, P., Reichstein, M., Baldocchi, D., Law, B. E., Papale, D., ... Wohlfahrt, G. (2009). Temporal and among-site variability of inherent water use efficiency at the ecosystem level. *Global Biogeochemical Cycles*, 23(2). <https://doi.org/10.1029/2008gb003233>
- Bennie, J., Kubin, E., Wiltshire, A., Huntley, B., & Baxter, R. (2010). Predicting spatial and temporal patterns of bud-burst and spring frost risk in north-west Europe: The implications of local adaptation to climate. *Global Change Biology*, 16, 1503–1514. <https://doi.org/10.1111/j.1365-2486.2009.02095.x>
- Bijleveld, C. C. J. H., van der Kamp, L. J. T., Mooijaart, A., van der Kloot, W. A., van der Leeden, R., & van der Burg, E. (1998). *Longitudinal data analysis: Designs, models and methods*. Thousand Oaks, CA: Sage Publications Ltd.
- Bonal, D., Bosc, A., Ponton, S., Goret, J., Burban, B., Gross, P., ... Granier, A. (2008). Impact of severe dry season on net ecosystem exchange in the Neotropical rainforest of French Guiana. *Global Change Biology*, 14, 1917–1933. <https://doi.org/10.1111/j.1365-2486.2008.01610.x>
- Brooks, S. P., & Gelman, A. (1998). General methods for monitoring convergence of iterative simulations. *Journal of Computational and Graphical Statistics*, 7, 434–455. <https://doi.org/10.1080/10618600.1998.10474787>

- Campbell, G. S. (1977). *An introduction to environmental biophysics*. New York, NY: Springer-Verlag. <https://doi.org/10.1007/bf02909456>
- Campbell, R. J., Marini, R. P., & Birch, J. B. (1992). Canopy position affects light response curves for gas exchange characteristics of apple spur leaves. *Journal of the American Society for Horticultural Science*, 117, 467–472. <https://doi.org/10.21273/JASHS.117.3.467>
- Clark, J. S. (2007). *Models for ecological data: An introduction*. Princeton, NJ: Princeton University Press.
- Dietze, M. C. (2017). *Ecological forecasting*. Princeton, NJ: Princeton University Press. Retrieved from <https://doi.org/10.1515/9781400885459>
- Drought 2018 Team, & ICOS Ecosystem Thematic Centre. (2019). *Drought-2018 ecosystem eddy covariance flux product in FLUXNET-archive format - Release 2019-1 (version 1.1)*. ICOS Carbon Portal. Retrieved from <https://doi.org/10.18160/pzdk-ef78>
- Efron, B. (1979). Computers and the theory of statistics: Thinking the unthinkable. *SIAM Review*, 21, 460–480. <https://doi.org/10.1137/1021092>
- Falge, E., Baldocchi, D., Tenhunen, J., Aubinet, M., Bakwin, P., Berbigier, P., ... Wofsy, S. (2002). Seasonality of ecosystem respiration and gross primary production as derived from FLUXNET measurements. *Agricultural and Forest Meteorology*, 113(1–4), 53–74. [https://doi.org/10.1016/s0168-1923\(02\)00102-8](https://doi.org/10.1016/s0168-1923(02)00102-8)
- Field, C. J. O. (1983). Allocating leaf nitrogen for the maximization of carbon gain: Leaf age as a control on the allocation program. *Oecologia*, 56, 341–347. <https://doi.org/10.1007/bf00379710>
- Gauch, H. G., Hwang, J. T., & Fick, G. W. (2003). Model evaluation by comparison of model-based predictions and measured values. *Agronomy Journal*, 95, 1442–1446. <https://doi.org/10.2134/agronj2003.1442>
- Gauch, H. G. Jr, Hwang, J. T. G., & Fick, G. (2004). Reply: Comments on another way of partitioning mean squared deviation proposed by Gauch et al (2003) (multiple letters). *Agronomy Journal*. <https://doi.org/10.2134/agronj2004.1206>
- Gebremichael, M., & Barros, A. P. (2006). Evaluation of MODIS Gross Primary Productivity (GPP) in tropical monsoon regions. *Remote Sensing of Environment*, 100, 150–166. <https://doi.org/10.1016/j.rse.2005.10.009>
- Gelman, A., & Rubin, D. B. (1992). Inference from iterative simulation using multiple sequences. *Statistical Science*, 7, 457–472. <https://doi.org/10.1214/ss/1177011136>
- Global Soil Data Task Group. (2000). *Global gridded surfaces of selected soil characteristics (IGBP-DIS)*. Oak Ridge, TN: ORNL DAAC. Retrieved from <https://doi.org/10.3334/ORNLDAAC/569>
- Grelle, A., Lundberg, A., Lindroth, A., Morén, A. S., & Cienciala, E. (1997). Evaporation components of a boreal forest: Variations during the growing season. *Journal of Hydrology*, 197(1–4), 70–87. [https://doi.org/10.1016/s0022-1694\(96\)03267-2](https://doi.org/10.1016/s0022-1694(96)03267-2)
- Hammer, G., & Wright, G. (1994). A theoretical analysis of nitrogen and radiation effects on radiation use efficiency in peanut. *Australian Journal of Agricultural Research*, 45, 575–589. <https://doi.org/10.1071/ar9940575>
- Hartig, F., Dyke, J., Hickler, T., Higgins, S. I., O'Hara, R. B., Scheiter, S., & Huth, A. (2012). Connecting dynamic vegetation models to data – An inverse perspective. *Journal of Biogeography*, 39, 2240–2252. <https://doi.org/10.1111/j.1365-2699.2012.02745.x>
- Hartig, F., Minunno, F., & Paul, S. (2017). *BayesianTools: General-purpose MCMC and SMC samplers and tools for Bayesian statistics*. R package version 0.1.4. <https://CRAN.R-project.org/package=BayesianTools>
- Hastings, W. K. (1970). Monte Carlo sampling methods using Markov chains and their applications. *Biometrika*, 57, 97–109. <https://doi.org/10.1093/biomet/57.1.97>
- Heinsch, F. A., Zhao, M., Running, S. W., Kimball, J. S., Nemani, R. R., Davis, K. J., ... Flanagan, L. B. (2006). Evaluation of remote sensing based terrestrial productivity from MODIS using regional tower eddy flux network observations. *IEEE Transactions on Geoscience and Remote Sensing*, 44, 1908–1925. <https://doi.org/10.1109/tgrs.2005.853936>
- Hollinger, D. Y., & Richardson, A. D. (2005). Uncertainty in eddy covariance measurements and its application to physiological models. *Tree Physiology*, 25, 873–885. <https://doi.org/10.1093/treephys/25.7.873>
- Kallioikoski, T., Mäkelä, A., Fronzek, S., Minunno, F., & Peltoniemi, M. (2018). Decomposing sources of uncertainty in climate change projections of boreal forest primary production. *Agricultural and Forest Meteorology*, 262, 192–205. <https://doi.org/10.1016/j.agrformet.2018.06.030>
- Kergoat, L., Lafont, S., Arneith, A., Le Dantec, V., & Saugier, B. (2008). Nitrogen controls plant canopy light-use efficiency in temperate and boreal ecosystems. *Journal of Geophysical Research: Biogeosciences*, 113(G4). <https://doi.org/10.1029/2007jg000676>
- Kirkham, M. B. (2014). *Principles of soil and plant water relations*. Boston, MA: Academic Press. Retrieved from <https://doi.org/10.1016/C2013-0-12871-1>
- Kobayashi, K. (2004). Comments on another way of partitioning mean squared deviation proposed by Gauch et al (2003). *Agronomy Journal*, 96(4), 1206–1207. <https://doi.org/10.2134/agronj2004.1206>
- Kobayashi, K., & Salam, M. U. (2000). Comparing simulated and measured values using mean squared deviation and its components research partly supported by Core Research for Evolutional Science and Technology (CREST) of Japan Science and Technology Corp. (JST). *Agronomy Journal*, 92, 345–352. <https://doi.org/10.2134/agronj2000.922345x>
- Kozlov, A., Kozlova, M., & Skorik, N. (2016). A simple harmonic model for FAPAR temporal dynamics in the wetlands of the Volga-Akhtuba floodplain. *Remote Sensing*, 8, 762. <https://doi.org/10.3390/rs8090762>
- Kuusisto, E. (1984). *Snow accumulation and snowmelt in Finland* (Vol. 55, pp. 1–149). Finland: Publications of Water Research Institute.
- Laloy, E., & Vrugt, J. A. (2012). High-dimensional posterior exploration of hydrologic models using multiple-try DREAM(ZS) and high-performance computing. *Water Resources Research*, 48. <https://doi.org/10.1029/2011wr010608>
- Lambers, H., Chapin, F. S., & Pons, T. L. (2008). Photosynthesis. In *Plant physiological ecology*. Germany: Springer Science & Business Media. Retrieved from <https://doi.org/10.1007/978-0-387-78341-3>
- Landsberg, J. (2003). Modelling forest ecosystems: State of the art, challenges, and future directions. *Canadian Journal of Forest Research*, 33, 385–397. <https://doi.org/10.1139/x02-129>
- Landsberg, J. J., & Sands, P. J. (2011). *Physiological ecology of forest production: Principles, processes and models*. Amsterdam, the Netherlands: Elsevier/Academic Press. Retrieved from <https://doi.org/10.1016/c2009-0-01727-9>
- Landsberg, J. J., & Waring, R. H. (1997). A generalised model of forest productivity using simplified concepts of radiation-use efficiency, carbon balance and partitioning. *Forest Ecology and Management*, 95, 209–228. [https://doi.org/10.1016/s0378-1127\(97\)00026-1](https://doi.org/10.1016/s0378-1127(97)00026-1)
- Leuning, R., Cromer, R. N., & Rance, S. (1991). Spatial distributions of foliar nitrogen and phosphorus in crowns of *Eucalyptus grandis*. *Oecologia*, 88, 504–510. <https://doi.org/10.1007/bf00317712>
- Lu, X., & Zhuang, Q. (2010). Evaluating evapotranspiration and water-use efficiency of terrestrial ecosystems in the conterminous United States using MODIS and AmeriFlux data. *Remote Sensing of Environment*, 114(9), 1924–1939. <https://doi.org/10.1016/j.rse.2010.04.001>
- Mäkelä, A. (1997). A carbon balance model of growth and self-pruning in trees based on structural relationships. *Forest Science*, 43(1), 7–24. <https://doi.org/10.1093/forestscience/43.1.7>
- Makela, A., Landsberg, J., Ek, A. R., Burk, T. E., Ter-Mikaelian, M., Agren, G. I., ... Puttonen, P. (2000). Process-based models for forest ecosystem management: Current state of the art and challenges for practical implementation. *Tree Physiology*, 20, 289–298. <https://doi.org/10.1093/treephys/20.5-6.289>
- Mäkelä, A., Pulkkinen, M., Kolari, P., Lagergren, F., Berbigier, P., Lindroth, A., ... Hari, P. (2008). Developing an empirical model of stand GPP

- with the LUE approach: Analysis of eddy covariance data at five contrasting conifer sites in Europe. *Global Change Biology*, 14, 92–108. <https://doi.org/10.1111/j.1365-2486.2007.01463.x>
- Marler, R. T., & Arora, J. S. (2010). The weighted sum method for multi-objective optimization: New insights. *Structural Multidisciplinary Optimization*, 41, 853–862. <https://doi.org/10.1007/s00158-009-0460-7>
- Martínez, B., Camacho, F., Verger, A., García-Haro, F. J., & Gilabert, M. A. (2013). Intercomparison and quality assessment of MERIS, MODIS and SEVIRI FAPAR products over the Iberian Peninsula. *International Journal of Applied Earth Observation and Geoinformation*, 21, 463–476. <https://doi.org/10.1016/j.jag.2012.06.010>
- Metropolis, N., Rosenbluth, A. W., Rosenbluth, M. N., Teller, A. H., & Teller, E. (1953). Equation of state calculations by fast computing machines. *The Journal of Chemical Physics*, 21, 1087–1092. <https://doi.org/10.2172/4390578>
- Minunno, F., Peltoniemi, M., Härkönen, S., Kallioikoski, T., Makinen, H., & Mäkelä, A. (2019). Bayesian calibration of a carbon balance model PREBAS using data from permanent growth experiments and national forest inventory. *Forest Ecology and Management*, 440, 208–257. <https://doi.org/10.1016/j.foreco.2019.02.041>
- Minunno, F., Peltoniemi, M., Launiainen, S., Aurela, M., Lindroth, A., Lohila, A., ... Mäkelä, A. (2016). Calibration and validation of a semi-empirical flux ecosystem model for coniferous forests in the Boreal region. *Ecological Modelling*, 341, 37–52. <https://doi.org/10.1016/j.ecolmodel.2016.09.020>
- Monserud, R. A. (2003). Evaluating forest models in a sustainable forest management context. *Forest Biometry, Modelling and Information Sciences*, 1, 35–47.
- Mooney, H. A., & Billings, W. D. (1961). Comparative physiological ecology of Arctic and Alpine populations of *Oxyria digyna*. *Ecological Monographs*, 31, 1–29. <https://doi.org/10.2307/1950744>
- Myneni, R., Knyazikhin, Y., & Park, T. (2015a). MOD15A2 MODIS/terra leaf area index/FPAR 8-day L4 global 1 km SIN grid. NASA LP DAAC. Retrieved from <https://doi.org/10.5067/MODIS/MOD15A2.006>
- Myneni, R., Knyazikhin, Y., & Park, T. (2015b). MOD15A2H MODIS/terra leaf area index/FPAR 8-day L4 global 500 m SIN grid V006. NASA EOSDIS Land Processes DAAC. Retrieved from <https://doi.org/10.5067/MODIS/MOD15A2H.006>
- Niu, S., Fu, Y., Gu, L., & Luo, Y. (2013). Temperature sensitivity of canopy photosynthesis phenology in northern ecosystems. In M. D. Schwartz (Ed.), *Phenology: An integrative environmental science*. Dordrecht, the Netherlands: Springer. Retrieved from [https://doi.org/10.1007/978-94-007-6925-0\\_27](https://doi.org/10.1007/978-94-007-6925-0_27)
- ORNL DAAC. (2008). MODIS collection 5 land products global subsetting and visualization tool. Oak Ridge, TN: ORNL DAAC. Retrieved from <https://doi.org/10.3334/ORNLDAAC/1241>
- ORNL DAAC. (2017). MODIS collection 6 land products global subsetting and visualization tool. Oak Ridge, TN: ORNL DAAC. Retrieved from <https://doi.org/10.3334/ORNLDAAC/1379>
- ORNL DAAC. (2018). MODIS and VIIRS land products global subsetting and visualization tool. Oak Ridge, TN: ORNL DAAC. Retrieved from <https://doi.org/10.3334/ORNLDAAC/1379>
- Papale, D., Reichstein, M., Aubinet, M., Canfora, E., Bernhofer, C., Kutsch, W., ... Yakir, D. (2006). Towards a standardized processing of net ecosystem exchange measured with eddy covariance technique: Algorithms and uncertainty estimation. *Biogeosciences*, 3, 571–583. <https://doi.org/10.5194/bg-3-571-2006>
- Peel, M. C., Finlayson, B. L., & McMahon, T. A. (2007). Updated world map of the Köppen-Geiger climate classification. *Hydrology and Earth System Sciences Discussions*, 4, 439–473. <https://doi.org/10.5194/hessd-4-439-2007>
- Pelletier, J. D., Broxton, P. D., Hazenberg, P., Zeng, X., Troch, P. A., Niu, G., ... Gochis, D. (2016). Global 1-km gridded thickness of soil, regolith, and sedimentary deposit layers. Oak Ridge, TN: ORNL DAAC. Retrieved from <https://doi.org/10.3334/ORNLDAAC/1304>
- Peltoniemi, M., Markkanen, T., Härkönen, S., Muukkonen, P., Thum, T., Aalto, T., & Mäkelä, A. (2015). Consistent estimates of gross primary production of Finnish forests – Comparison of estimates of two process models. *Boreal Environment Research*, 20, 196–212.
- Peltoniemi, M., Pulkkinen, M., Aurela, M., Pumpanen, J., Kolari, P., & Mäkelä, A. (2015). A semi-empirical model of boreal-forest gross primary production, evapotranspiration, and soil water – Calibration and sensitivity analysis. *Boreal Environment Research*, 20, 151–171. <https://doi.org/10.5194/gmdd-8-5089-2015>
- Peltoniemi, M., Pulkkinen, M., Kolari, P., Duursma, R. A., Montagnani, L., Wharton, S., ... Mäkelä, A. (2012). Does canopy mean nitrogen concentration explain variation in canopy light use efficiency across 14 contrasting forest sites? *Tree Physiology*, 32, 200–218. <https://doi.org/10.1093/treephys/tptr140>
- Potter, C. S., Randerson, J. T., Field, C. B., Matson, P. A., Vitousek, P. M., Mooney, H. A., & Klooster, S. A. (1993). Terrestrial ecosystem production: A process model based on global satellite and surface data. *Global Biogeochemical Cycles*, 7, 811–841. <https://doi.org/10.1029/93gb02725>
- Rahman, M. M., & Tsukamoto, J. (2013). Leaf traits, litter decomposability and forest floor dynamics in an evergreen- and a deciduous-broad-leaved forest in warm temperate Japan. *Forestry*, 86, 441–451. <https://doi.org/10.1093/forestry/cpt015>
- Reichstein, M., Falge, E., Baldocchi, D., Papale, D., Aubinet, M., Berbigier, P., ... Valentini, R. (2005). On the separation of net ecosystem exchange into assimilation and ecosystem respiration: Review and improved algorithm. *Global Change Biology*, 11, 1424–1439. <https://doi.org/10.1111/j.1365-2486.2005.001002.x>
- Richardson, A. D., Mahecha, M. D., Falge, E., Kattge, J., Moffat, A. M., Papale, D., ... Hollinger, D. Y. (2008). Statistical properties of random CO<sub>2</sub> flux measurement uncertainty inferred from model residuals. *Agricultural and Forest Meteorology*, 148, 38–50. <https://doi.org/10.1016/j.agrformet.2007.09.001>
- Running, S. W., & Coughlan, J. C. (1988). A general model of forest ecosystem processes for regional applications I. Hydrologic balance, canopy gas exchange and primary production processes. *Ecological Modelling*, 42(2), 125–154. [https://doi.org/10.1016/0304-3800\(88\)90112-3](https://doi.org/10.1016/0304-3800(88)90112-3)
- Running, S. W., Nemani, R., Glassy, J. M., & Thornton, P. E. (1999). MODIS daily photosynthesis (PSN) and annual net primary production (NPP) product (MOD17): Algorithm theoretical basis document. University of Montana, SCF At-Launch Algorithm ATBD Documents.
- Running, S., Mu, Q., & Zhao, M. (2015). MOD17A2H MODIS/terra gross primary productivity 8-day L4 global 500 m SIN grid V006. NASA EOSDIS Land Processes DAAC. Retrieved from <https://doi.org/10.5067/MODIS/MOD17A2H.006>
- Running, S. W., Nemani, R. R., Heinsch, F. A., Zhao, M., Reeves, M., & Hashimoto, H. (2004). A continuous satellite-derived measure of global terrestrial primary production. *BioScience*, 54, 547–560. [https://doi.org/10.1641/0006-3568\(2004\)054\[0547:acsmog\]2.0.co;2](https://doi.org/10.1641/0006-3568(2004)054[0547:acsmog]2.0.co;2)
- Saldarriaga, J. G., & Luxmoore, R. J. (1991). Solar energy conversion efficiencies during succession of a tropical rain forest in Amazonia. *Journal of Tropical Ecology*, 7, 233–242. <https://doi.org/10.1017/s0266467400005393>
- Schenk, H. J., & Jackson, R. B. (2009). ISLSCP II Ecosystem rooting depths. Oak Ridge, TN: ORNL DAAC. Retrieved from <https://doi.org/10.3334/ORNLDAAC/929>
- Sims, D., Rahman, A., Cordova, V., Elmasri, B., Baldocchi, D., Bolstad, P., ... Misson, L. (2008). A new model of gross primary productivity for North American ecosystems based solely on the enhanced vegetation index and land surface temperature from MODIS. *Remote Sensing of Environment*, 112, 1633–1646. <https://doi.org/10.1016/j.rse.2007.08.004>

- Sivia, D., & Skilling, J. (2006). *Data analysis: A Bayesian tutorial*. Oxford, UK: Oxford University Press.
- Theil, H. (1966). *Applied economic forecasting*. Amsterdam, the Netherlands: North Holland Publishing Company. Retrieved from <https://doi.org/10.2307/2229320>
- Valentine, H. T., & Mäkelä, A. (2005). Bridging process-based and empirical approaches to modeling tree growth. *Tree Physiology*, 25(7), 769–779. <https://doi.org/10.1093/treephys/25.7.769>
- Van Oijen, M. (2017). Bayesian methods for quantifying and reducing uncertainty and error in forest models. *Current Forestry Reports*, 3, 269–280. <https://doi.org/10.1007/s40725-017-0069-9>
- Van Oijen, M., Rougier, J., & Smith, R. (2005). Bayesian calibration of process-based forest models: Bridging the gap between models and data. *Tree Physiology*, 25, 915–927. <https://doi.org/10.1093/treephys/25.7.915>
- Vrugt, J. A., ter Braak, C. J. F., Diks, C. G. H., Robinson, B. A., Hyman, J. M., & Higdon, D. (2009). Accelerating Markov chain Monte Carlo simulation by differential evolution with self-adaptive randomized subspace sampling. *International Journal of Nonlinear Sciences and Numerical Simulation*, 10(3), 273–290. <https://doi.org/10.1515/ijnsns.2009.10.3.273>
- Ware, J., & Liang, K. (1996). The design and analysis of longitudinal studies: A historical perspective. *Advances in Biometry*, 1996, 339–362.
- Waring, R. H., Coops, N. C., & Landsberg, J. J. (2010). Improving predictions of forest growth using the 3-PGS model with observations made by remote sensing. *Forest Ecology and Management*, 259, 1722–1729. <https://doi.org/10.1016/j.foreco.2009.05.036>
- Weiskittel, A. R., Hann, D. W., Kershaw, J. A. Jr, & Vanclay, J. K. (2011). *Forest growth and yield modeling*. New York, NY: John Wiley and Sons, Inc. Retrieved from <https://doi.org/10.1002/978111998518>
- Yuan, W., Cai, W., Liu, S., Dong, W., Chen, J., Arain, M. A., ... Xia, J. (2014). Vegetation-specific model parameters are not required for estimating gross primary production. *Ecological Modelling*, 292, 1–10. <https://doi.org/10.1016/j.ecolmodel.2014.08.017>
- Yuan, W., Cai, W., Xia, J., Chen, J., Liu, S., Dong, W., ... Wohlfahrt, G. (2014). Global comparison of light use efficiency models for simulating terrestrial vegetation gross primary production based on the LaThuile database. *Agricultural and Forest Meteorology*, 192–193, 108–120. <https://doi.org/10.1016/j.agrformet.2014.03.007>
- Yuan, W., Liu, S., Zhou, G., Zhou, G., Tieszen, L. L., Baldocchi, D., ... Wofsy, S. C. (2007). Deriving a light use efficiency model from eddy covariance flux data for predicting daily gross primary production across biomes. *Agricultural and Forest Meteorology*, 143, 189–207. <https://doi.org/10.1016/j.agrformet.2006.12.001>
- Zheng, Y., Zhang, L., Xiao, J., Yuan, W., Yan, M., Li, T., & Zhang, Z. (2018). Sources of uncertainty in gross primary productivity simulated by light use efficiency models: Model structure, parameters, input data, and spatial resolution. *Agricultural and Forest Meteorology*, 263, 242–257. <https://doi.org/10.1016/j.agrformet.2018.08.003>

## SUPPORTING INFORMATION

Additional supporting information may be found online in the Supporting Information section.

**How to cite this article:** Tian X, Minunno F, Cao T, Peltoniemi M, Kalliokoski T, Mäkelä A. Extending the range of applicability of the semi-empirical ecosystem flux model PRELES for varying forest types and climate. *Glob Change Biol*. 2020;26:2923–2943. <https://doi.org/10.1111/gcb.14992>